Article

Cell

Higher-Order Clustering of the Transmembrane Anchor of DR5 Drives Signaling

Graphical Abstract

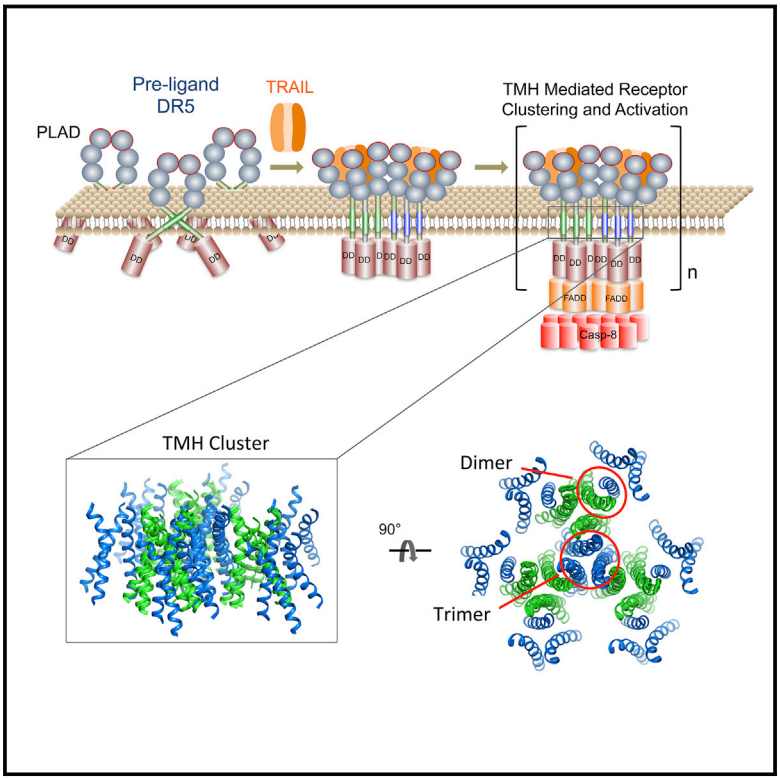

Authors

Liqiang Pan, Tian-Min Fu, Wenbin Zhao, ..., Shuqing Chen, Hao Wu, James J. Chou

Correspondence

chenshuqing@zju.edu.cn (S.C.), wu@crystal.harvard.edu (H.W.), james_chou@hms.harvard.edu (J.J.C.)

In Brief

Unlike traditional receptor clustering mediated by intracellular and extracellular domain oligomerization, the transmembrane domain alone of some TNF family receptors can form higher-order structures competent to drive signaling, basally inhibited by the unliganded ectodomain.

Highlights

- Transmembrane helix of death receptor 5 oligomerizes to drive downstream signaling
- The transmembrane helix in lipid bilayer forms dimer-trimer interaction network
- Receptor ectodomain in pre-ligand state inhibits receptor clustering and activation
- Ligand binding overcomes the pre-ligand autoinhibition

Pan et al., 2019, Cell *176*, 1477–1489
March 7, 2019 © 2019 Elsevier Inc.
https://doi.org/10.1016/j.cell.2019.02.001

CellPress

Article

Cell

Higher-Order Clustering of the Transmembrane Anchor of DR5 Drives Signaling

Liqiang Pan,[1,5] Tian-Min Fu,[1,2,5] Wenbin Zhao,[3,5] Linlin Zhao,[1,5] Wen Chen,[1] Chixiao Qiu,[3] Wenhui Liu,[3] Zhijun Liu,[4] Alessandro Piai,[1] Qingshan Fu,[1] Shuqing Chen,[3,*] Hao Wu,[1,2,*] and James J. Chou[1,6,*]

[1]Department of Biological Chemistry and Molecular Pharmacology, Blavatnik Institute at Harvard Medical School, 250 Longwood Avenue, Boston, MA 02115, USA

[2]Program in Cellular and Molecular Medicine, Boston Children's Hospital, Boston, MA 02115, USA

[3]Institute of Drug Metabolism and Pharmaceutical Analysis and Zhejiang Province Key Laboratory of Anti-cancer Drug Research, College of Pharmaceutical Sciences, Zhejiang University, 310058 Hangzhou, China

[4]National Facility for Protein Science in Shanghai, ZhangJiang Lab, Chinese Academy of Sciences, 201210 Shanghai, China

[5]These authors contributed equally

[6]Lead Contact

*Correspondence: chenshuqing@zju.edu.cn (S.C.), wu@crystal.harvard.edu (H.W.), james_chou@hms.harvard.edu (J.J.C.)

https://doi.org/10.1016/j.cell.2019.02.001

SUMMARY

Receptor clustering on the cell membrane is critical in the signaling of many immunoreceptors, and this mechanism has previously been attributed to the extracellular and/or the intracellular interactions. Here, we report an unexpected finding that for death receptor 5 (DR5), a receptor in the tumor necrosis factor receptor superfamily, the transmembrane helix (TMH) alone in the receptor directly assembles a higher-order structure to drive signaling and that this structure is inhibited by the unliganded ectodomain. Nuclear magnetic resonance structure of the TMH in bicelles shows distinct trimerization and dimerization faces, allowing formation of dimer-trimer interaction networks. Single-TMH mutations that disrupt either trimerization or dimerization abolish ligand-induced receptor activation. Surprisingly, proteolytic removal of the DR5 ectodomain can fully activate downstream signaling in the absence of ligand. Our data suggest a receptor activation mechanism in which binding of ligand or antibodies to overcome the pre-ligand autoinhibition allows TMH clustering and thus signaling.

INTRODUCTION

Members of the tumor necrosis factor receptor superfamily (TNFRSF) can be specifically activated to induce death of many cancer cells or regulate proliferation and activation of immune cells (Ashkenazi and Dixit, 1998; Boldin et al., 1995; Nagata and Golstein, 1995; Rieux-Laucat et al., 1995; Watts, 2005). There are genuine needs for in-depth understanding of the mechanism by which these receptors are activated, as many of them are targets for antibody-based activation for cancer therapy, e.g., the immune cell co-stimulators 4-1BB, OX40, and BCMA of the TNFRSF in immune-oncology (Cooper et al., 2002; Hatzoglou et al., 2000; Rogers et al., 2001), as well as death receptor 5 (DR5, also known as TRAIL receptor 2) in tumor killing by the extrinsic pathway of caspase activation (Ashkenazi, 2008; Chaudhary et al., 1997; Sheridan et al., 1997).

Receptors in the TNFRSF are type I transmembrane (TM) proteins with an extracellular domain (ECD) composed of multiple cysteine-rich domains (CRDs), a transmembrane helix (TMH), and an intracellular region that specifically interact with signaling adaptors such as Fas-associated death domain (FADD), TNFR1-associated death domain (TRADD), or TNFR-associated factor (TRAFs) (Baker and Reddy, 1998). Early functional and structural studies on TNFR1 and Fas have painted an overall picture of receptor triggering by trimerization (Vanamee and Faustman, 2018; Wajant, 2002). The binding of the trimeric ligand, in which neighboring protomers of the ligand interact with a receptor ECD, causes the receptor to trimerize. It is presumed that ECD trimerization allows subsequent clustering of the intracellular domains that recruits and activates downstream signaling proteins. In the case of Fas, structural studies of its intracellular death domain (DD) in complex with FADD suggested formation of a higher-order oligomeric signaling complex (Esposito et al., 2010; Wang et al., 2010).

More recently, we showed that the Fas TMH forms a trimer with a proline-containing signature sequence that allows for close van der Waals (VDW) contacts between the protomers (Fu et al., 2016). Disruptive mutations for TMH trimer formation severely attenuated Fas ligand (FasL)-induced signaling (Fu et al., 2016) and several of these mutations are oncogenic in human (Grønbaek et al., 1998; Lee et al., 2000). These results suggest that TMH trimerization positions the Fas intracellular DD in the right arrangement to cluster and form the so-called death-inducing signaling complex (DISC) with FADD and caspase-8 (Driscoll, 2014). In contrast, none of the mutations that disrupted the TMH trimer had any effect on receptor self-association in the absence of FasL, suggesting that the TMH associates differently in the pre-ligand state of the receptor or does not participate in pre-ligand association (Fu et al., 2016). In this regard, previous studies suggested that the N-terminal CRD1 of TNFR1, Fas, and other TNFRSF family members form a pre-ligand association domain (PLAD) and that a signaling defective mutant receptor with an intact PLAD dominant-negatively

inhibits signaling by the wild-type (WT) receptor (Chan, 2007; Chan et al., 2000; Siegel et al., 2000b).

The molecular mechanism for TNFRSF signaling remains intriguing, especially with respect to the TMH. First, while existing models propose that ligand- and antibody-induced clustering at the ECD activates intracellular signaling (Vanamee and Faustman, 2018), how can different ligands such as trimeric TNF family members and dimeric nerve growth factor (NGF) and antibodies with potentially different clustering geometries all position the TMH for activation is unexplained. Second, while the proline motif found to mediate TMH trimerization in Fas is present in many members of the TNFRSF such as TNFR1, DR3, DR4, and CD40, it is absent in several other members such as DR5, OX40, and 4-1BB (Table S1). Instead, the TMHs of DR5 and OX40, for example, contain the GXXXG motif known for mediating TMH dimerization, not trimerization (MacKenzie et al., 1997; Trenker et al., 2015). Third, the oligomeric state of pre-ligand receptor association has been debated between dimeric (Naismith et al., 1995; Vanamee and Faustman, 2018) and trimeric (Valley et al., 2012), although there is not yet direct evidence for either form.

In this study, we performed structural and functional investigation on the DR5 TMH ($DR5^{TMH}$) to address the above issues while potentially uncovering previously unrecognized roles of TMH in receptor signaling. We determined the NMR structure of $DR5^{TMH}$ in the lipid-bilayer environment of small bicelles, which surprisingly showed distinct surfaces for both dimeric and trimeric interactions, via the GXXXG motif and a non-proline motif, respectively. On the cell membrane, these interfaces together should allow DR5 to form a supramolecular dimer-trimer network to mediate higher-order clustering and signaling. Further cell-based functional studies revealed that the ECD is not required for DR5 signaling; the intrinsic dimer-trimer network of TMH alone is both necessary and sufficient to drive DR5-mediated cell death, while unliganded ECD inhibits TMH oligomerization. These results challenge the view that ligand-induced extracellular clustering initiates the signaling but rather suggest the postulation that an important role of ligand binding is to overcome ECD autoinhibition on the TMH. This hypothesis provides a unified explanation for the long-standing question on how both dimeric and trimeric binders activate TNFRSF signaling because unlike specific positioning, relieving autoinhibition may not require a specific clustering geometry. Furthermore, structure-based dimer-specific mutagenesis of the TMH, but not trimer-specific mutagenesis, significantly affects pre-ligand receptor association, which provides direct evidence not only for a dimeric pre-ligand state but also for participation of TMH in this process as well.

RESULTS

DR5 TMH Contains Both Trimer and Dimer Interfaces

We first investigated TMH assembly of DR5 using NMR and biochemistry protocols as similarly performed previously for the Fas TMH (Fu et al., 2016). DR5 has a domain organization similar to that of Fas; it contains an ECD composed of three CRDs, a TMH, and an intracellular DD (Figure 1A). While both ECD and DD are homologous between DR5 and Fas, the TMHs of the two death receptors share no recognizable sequence similarity. For NMR studies, we used a DR5 fragment from human isoform 1, containing residues 208–242, which encompasses the common predicted TMH of both isoforms (Figure S1A). The purified fragment, designated $DR5^{TMH}$, was reconstituted into bicelles with [lipid]/[detergent] ratio (q) of ~0.55 (Figures S1B and S1C). At this q, the estimated diameter of the bilayer region of the bicelle is ~49 Å (Glover et al., 2001; Sanders et al., 1994), and the proteins are in near lipid-bilayer environment (Piai et al., 2017b). We found that the unreconstituted $DR5^{TMH}$ migrated in SDS-PAGE primarily as a monomer (theoretical molecular weight [MW] 3.6 kDa; apparent MW ~5 kDa), while bicelle-reconstituted $DR5^{TMH}$ appeared in the gel as a trimer without crosslinking (apparent MW ~16 kDa) (Figure S1D). The WT $DR5^{TMH}$ bicelle sample generated high-quality NMR spectra (Figure S1E), indicating the TMH was well folded in bicelles, followed by successful backbone assignment of $DR5^{TMH}$ (Figure 1B).

Next, an isotopically mixed sample containing 1:1 mixture of (^{15}N, ^{2}H)-labeled $DR5^{TMH}$ and (15% ^{13}C)-labeled $DR5^{TMH}$ was used to exclusively detect inter-monomer nuclear Overhauser enhancements (NOEs) between the amide protons (H_N) of the deuterated monomers and the aliphatic protons of the fully protonated monomers. This experiment provided direct evidence of inter-monomer contacts in $DR5^{TMH}$ homo-oligomers. Unlike Fas^{TMH}, however, which showed inter-monomer NOEs for only one face of the TMH (Fu et al., 2016), $DR5^{TMH}$ showed too many NOEs on all sides of the helix that were not possible to fit with any trimer structures (Figure 1C). Among these NOEs, two were characterized to be from the backbone H_N of the two glycines (G213, G217) in the GXXXG motif to the $H\alpha$ of the same glycines on the opposite chain, respectively, indicating close glycine packing that is the structural hallmark of GXXXG-mediated TMH dimerization. Collectively, these NOE data suggested that both dimer and trimer interfaces existed in $DR5^{TMH}$ oligomers in bicelles, and that an obvious way to deconvolute the dimer- and trimer-specific NOEs was to generate a G217Y mutation in the GXXXG motif.

High-quality NMR spectra of the $DR5^{TMH}$ G217Y mutant suggest its well-folded structure, and its backbone was also assigned (Figures 1D and S2). Indeed, upon introducing the G217Y mutation, about half of the inter-monomer NOEs vanished, including GXXXG motif-associated NOEs (Figures 1E and 2A–2C), and the mutant still migrated in SDS-PAGE as a trimer (Figure 2D). The mutant results suggested that the single mutation in the GXXXG motif has removed the dimer interface but not the trimer interface. But, the exact oligomeric state of the WT and mutant $DR5^{TMH}$ was still unclear, because both appeared in SDS-PAGE as trimers (Figure 2D), whereas minimally hexamers were expected for the WT having both dimeric and trimeric interactions. Since SDS can be disruptive for certain TM helix assembly, we examined $DR5^{TMH}$ oligomeric state using an oligomer-labeling technique (OG-label) that we developed recently (Chen et al., 2018). In this method, each of the protomers in the bicelle-reconstituted His-tagged $DR5^{TMH}$ oligomer was labeled stoichiometrically with a TriNTA-tagged soluble crosslinkable protein (SCP) named GB1 via a His-NTA (nitrilotriacetic acid) interaction. The SCPs were then crosslinked with an

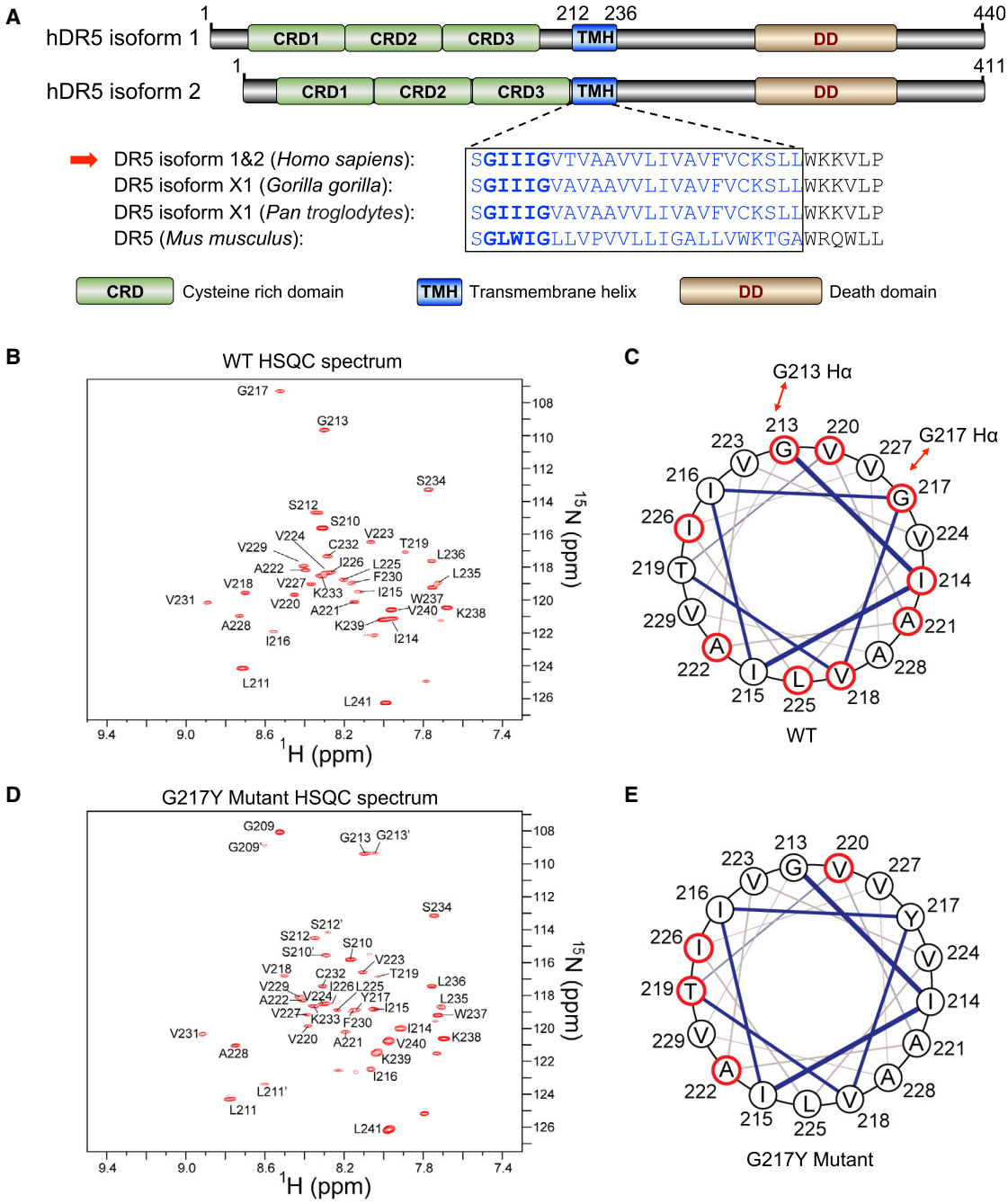

Figure 1. Presence of Dimer and Trimer Interfaces in the DR5 TMH Reconstituted in Bicelles with q = 0.55

(A) $DR5^{TMH}$ sequences from various species with the conserved GXXXG motif highlighted in boldface. The TMH is shown in the context of the overall domain organization of DR5.

(B) Spectra of the WT $DR5^{TMH}$. The ^{1}H-^{15}N TROSY-HSQC spectrum was recorded at ^{1}H frequency of 750 MHz using (^{15}N, ^{2}H)-labeled protein. See Figures S2A and S2B for ^{1}H-^{13}C TROSY-HSQC spectrum.

(C) Residues of the DR5 TMH in helical wheel representation that show inter-protomer contacts. The red circles indicate residues whose amide protons show inter-protomer NOEs with aliphatic protons (see Figure 2A for NOE data). The NOE data were collected in 1,2-dimyristoyl-sn-glycero-3-phosphocholine / 1,2-dihexanoyl-sn-glycero-3-phosphocholin (DMPC-DHPC) bicelles (q = 0.55).

(D) Spectra of the G217Y mutant recorded in the way as in (A) but at 800 MHz. The labels with apostrophes indicate the presence of a minor population for residues close to the N terminus. See Figure S2C for comparison of the $^{13}C\alpha$ secondary chemical shifts between the WT and the G217Y mutant.

(E) Same as in (B) except G217 is mutated to tyrosine (see Figures 2B and 2C for NOE data), showing disappearance of about half of the inter-protomer NOEs. See also Figure S2 and Table S1.

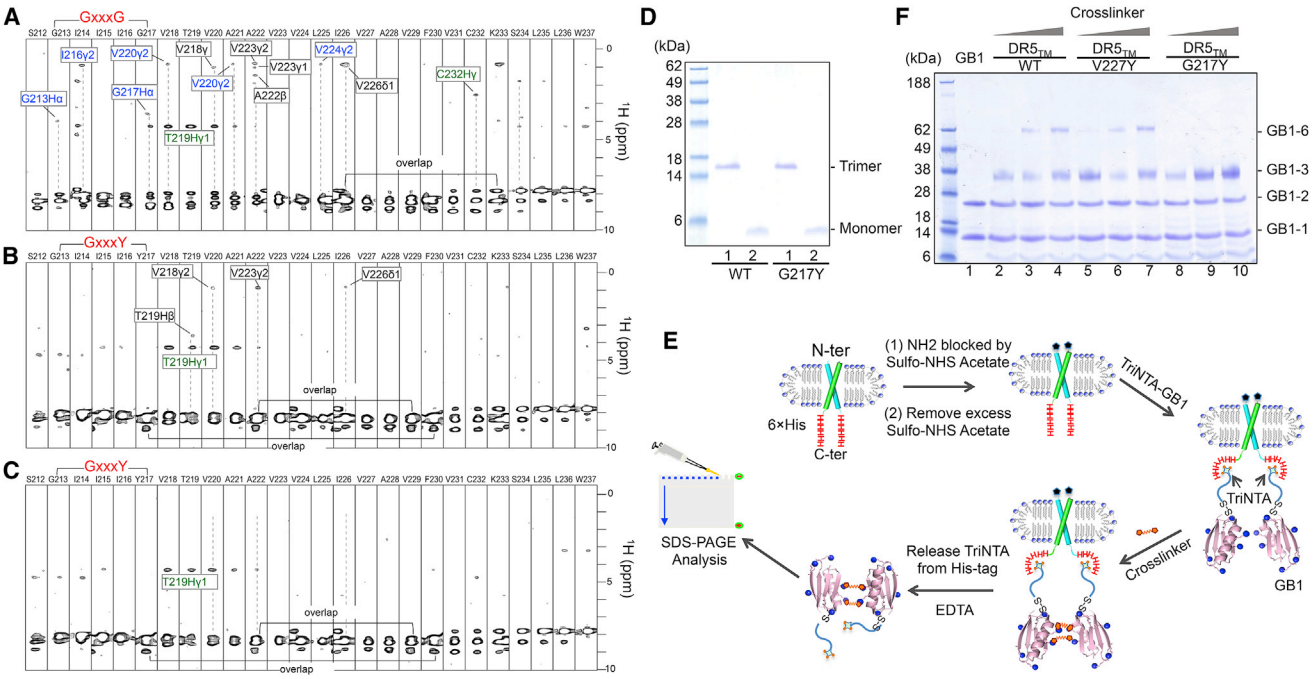

Figure 2. GXXXG Motif Mediated Minimal Dimer-Trimer Assembly of DR5^{TMH}

(A) Inter-protomer NOEs from the WT DR5^{TMH}. Strips from 3D ^{15}N-edited NOESY-TROSY-HSQC (τ_{NOE} = 200 ms) spectra were recorded using an isotopically mixed sample, consisting of 0.4 mM (^{15}N, ^{2}H)-labeled DR5^{TMH} and 0.4 mM (15% ^{13}C)-labeled DR5^{TMH}, premixed at the cell level before cell lysis and protein purification. The spectrum was recorded at ^{1}H frequency of 900 MHz. The assignment of NOE cross peaks from the dimer interface (blue) and from the trimer interface (black) was possible using the NOE data of the G217Y mutant that eliminated the dimer interface (see B and C). Peaks are labeled in green are due to labile (or exchangeable) protons.

(B) Inter-protomer NOEs from the G217Y mutant. The NOE data were collected and assigned as in (A) except the spectrum was recorded at ^{1}H frequency of 800 MHz.

(C) The negative control sample for (B) containing only 0.4 mM (^{15}N, ^{2}H)-labeled G217Y mutant. The spectrum was recorded exactly the same way as in (B).

(D) Oligomerization of DR5^{TMH} in bicelles analyzed by standard SDS-PAGE. The gel lanes from left to right are (1) purified WT DR5^{TMH} or the G217Y mutant reconstituted in bicelles, powder dissolved in gel loading buffer, and (2) pure WT DR5^{TMH} or the G217Y mutant powder dissolved in gel loading buffer. Samples were run under non-denaturing conditions (mixed with loading buffer and loaded onto the gel without boiling).

(E) Schematic illustration of the OG-label method for determining the oligomeric state of DR5^{TMH} in bicelles (Chen et al., 2018).

(F) Oligomerization of DR5^{TMH} analyzed by the OG-label method, which preserves the native state of the TMD assembly in bicelles (see STAR Methods).

See also Figure S2 and Table S2.

amine-reactive crosslinker (Lomant's reagent) and released from the DR5^{TMH} by EDTA for SDS-PAGE analysis (Figure 2E). The OG-label results clearly indicate that WT DR5^{TMH} in bicelles forms hexamers, whereas the G217Y mutant only forms trimers (Figure 2F). The same analysis also showed that the V227Y mutation, which was later shown to affect neither trimeric nor dimeric interaction, is also hexameric, as the WT (Figure 2F).

Atomic Structure of a Minimal Dimer-Trimer Assembly of DR5^{TMH}

To define both the trimerization and dimerization interfaces in the TMH assembly, we first determined the trimer structure of the G217Y mutant (Table S2). The NOE data of isotopically mixed DR5^{TMH} mutant showed obvious inter-monomer NOEs at T219, A222, and I226 (Figure 2B), resulting from trimeric packing at these positions. In parallel, a control sample with only (^{15}N, ^{2}H)-labeled protein did not generate the above NOEs (Figure 2C), confirming that the inter-monomer NOEs have arisen from mixing of differently labeled protomers. The trimer structure shows three layers of hydrophobic interaction along the 3-fold axis, including interactions between T219 and V218, between A222 and V223, and between I226 and L225 (Figures 3A and S3). Single mutations that were predicted by the structure to disrupt trimerization, T219Y and A222Y, both led to dissociation of the trimer (Figure 3B). The NMR structure of the G217Y mutant has a similar mode of trimerization as that of Fas^{TMH} (Fu et al., 2016), but with less intimate associations along the symmetry axis due to the lack of the proline motif (Figure 3C).

Having identified the trimer-specific inter-monomer contacts in the G217Y mutant, we were able to unambiguously assign both dimer- and trimer-specific NOEs in WT DR5^{TMH} (Figure 2A) and determined the minimal hexamer structure of DR5^{TMH} in bicelles (Figures 4A, S4A, and S4B). The trimeric assembly is essentially the same as that of the mutant. As expected, the dimerization interface mainly involves strong inter-monomer contacts at G213 and G217, although several other residues such as V220 and A221 appear to contribute as well with less

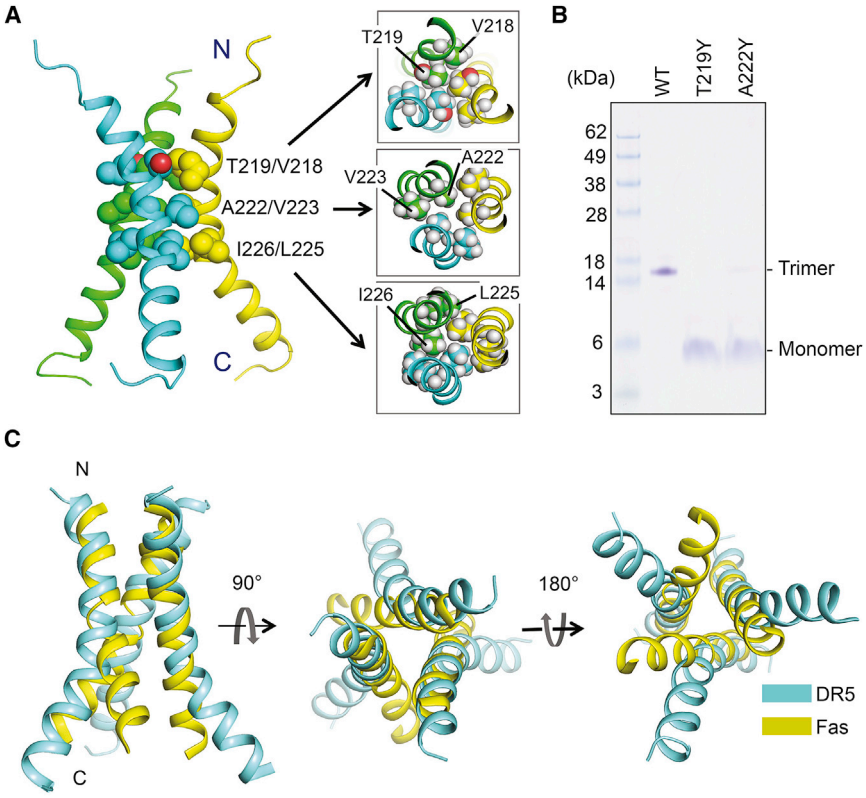

Figure 3. Structure of the Trimeric Interfaces of Human DR5^{TMH} in Bicelles

(A) Ribbon representation (left) of the trimeric G217Y mutant TMD with core residues highlighted (side-chain heavy atoms shown as spheres). The side-chain packing at three different levels along the TM helices is further illustrated with sectional top views of the trimer (right) (side-chain heavy atoms and protons included).

(B) SDS-PAGE analysis of several trimer-breaking mutations, introduced on top of the dimer-breaking G217Y mutation. Samples were run under a non-denaturing condition (DR5^{TMH} variants were reconstituted into bicelles, mixed with loading buffer, and loaded to the gel without boiling).

(C) Comparison between the TMH structures of human DR5 and Fas. The ribbon representations of DR5 and Fas TMHs are shown in cyan and yellow, respectively. The structural overlay shows that the Fas TMH trimer is overall more intimate than the DR5 TMH trimer.

See also Figure S3.

tight packing (Figure 4B). The OG-label analysis in Figure 2F already showed that the G217Y mutation can completely break the dimeric interaction. We note that our NOE data are consistent with either dimer-of-trimer or trimer-of-dimer model, as either would fit the bicelle size we used. The trimer-of-dimer structure was also calculated using the same set of NOE restraints (Figure S4C). Further, the fact that only one set of NMR peaks was observed in the transverse relaxation optimized spectroscopy-heteronuclear single-quantum correlation spectroscopy (TROSY-HSQC) spectrum (Figure 1B) is more consistent with a mixture of dimer-of-trimer and trimer-of-dimer in fast change.

To address the positions of the dimer- and trimer- forming residues in membrane, we performed TM partition analysis of the TMH using a paramagnetic probe titration (PPT) method developed previously for bicelle-reconstituted protein samples (Piai et al., 2017b). To simplify analysis, the trimeric mutant in bicelles was used because it only has one symmetry axis. Titration of the water-soluble paramagnetic probe Gd-DOTA outside the bicelles provided residue-specific paramagnetic relaxation enhancement amplitudes (PRE_{amp}) (Figure S4D). Then, PRE_{amp} versus *residue number* was converted to PRE_{amp} versus *position* (Figure S4E) by translating residue number to the corresponding H_N position along the 3-fold axis in the mutant structure. Finally, the TMH position relative to the bilayer center was determined using "sigmoidal fitting" (Figure S4F). The results indicate that the trimer-forming residues are mostly in the core of the bilayer, whereas the GXXXG motif is in the lipid head group region (Figure 4C).

Propagation of Dimerization and Trimerization Mediates Higher-Order Assembly of DR5

The estimated diameter of ~50 Å for the bilayer region of the bicelles used in DR5^{TMH} reconstitution for NMR studies would be able to fit either a dimer-of-trimer of the TMH or a trimer-of-dimer. However, in the absence of size restraints on the cell surface, having both trimeric and dimeric interfaces suggest that DR5^{TMH} is able to form higher-order clusters in membrane (Figures 4D and 4E). Indeed, superimposing one dimer in a trimer-of-dimers structure with a dimer in another trimer-of-dimers structure did not create any steric hindrance but rather generated multiple trimer-of-dimers (Figure 4D) that can mediate formation of a patch of dimer-trimer TMH network on membrane (Figure 4E).

TMH Clustering Is Required for DR5 Signaling

From the structure and mutagenesis data above, we identified a set of single-point mutations critical for addressing which TMH oligomerization is needed for DR5 activation, whether it is trimerization, dimerization, or both. These mutations are the dimer-breaking G217Y, the trimer-breaking T219Y or A222Y, and the control V227Y that has no effect on dimerization or trimerization. Moreover, the NMR structure explained why the mutation V227Y did not affect DR5^{TMH} oligomerization (Figure 2F) because V227 is not located in the dimer or trimer interface (Figure 5A). We tested these mutants with two independent experiments. The soluble DR5 ligand, known as TNF-related apoptosis-inducing ligand (TRAIL), was used to induce DR5-mediated apoptosis. In one case, the WT and mutants were transiently expressed in DR5-deficient BJAB cells in the form of C-terminal EGFP fusion proteins, and caspase-8 activity was monitored for TRAIL-induced receptor activity. Transfection efficiency was 40%–60% for all DR5 variants (Figure S5A), and the

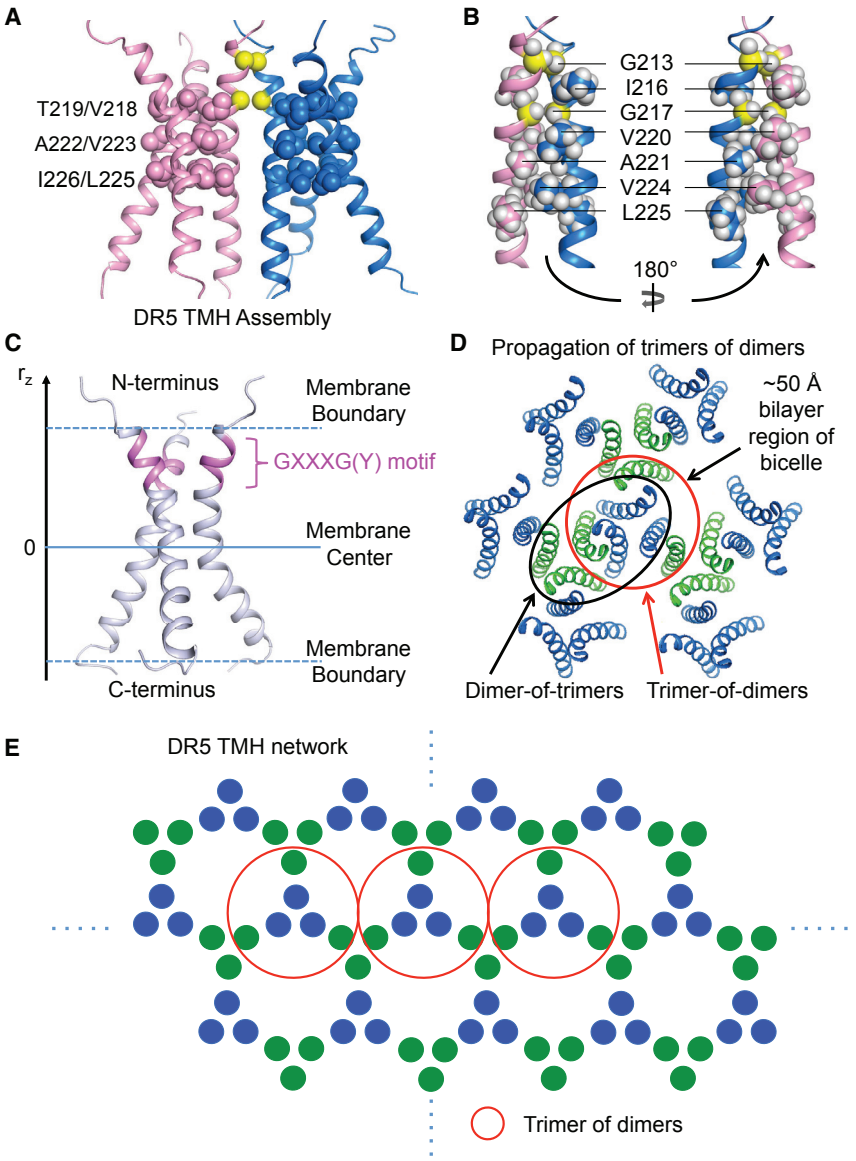

Figure 4. Propagation of Dimerization and Trimerization Mediates Higher-Order Assembly of DR5

(A) Ribbon representation of the dimer-of-trimer structure of the WT $DR5^{TMH}$. Residues involved in the trimer-specific inter-protomer contacts are highlighted (side-chain heavy atoms shown as spheres). In addition, the Cα atoms of G213 and G217 are shown as yellow spheres. Although the dimer-of-trimer model is calculated using the intermolecular NOE restraints, a trimer-of-dimer in the bicelle is also possible (see Figure S4C).

(B) Close-up view of the residues involved in the dimer-specific inter-protomer contacts (side-chain heavy atoms and protons shown as spheres).

(C) Transmembrane partition of the G217Y mutant trimer determined by the PPT method (Figures S4D–S4F), showing the positions of the trimerization core and the GXXXG motif relative to the lipid bilayer.

(D) Higher-order assembly model of DR5 mediated by propagation of dimerization and trimerization. Fitting multiple dimer-of-trimer structures from Figure 4A into the network, demonstrating the possibility of such network without steric clash. Red and black circles represent trimer-of-dimer and dimer-of-trimer unit, respectively, in the clustering network. Both of them fits in the lipid bilayer region of bicelle (q = 0.55, ~50 Å diameter).

(E) Schematic illustration of potential clustering network mediated by DR5 TMH, which contains both dimer and trimer interfaces. Representative trimer-of-dimer cluster units are labeled with red circle.

See also Figure S4.

receptors were mainly expressed on the cell surface (Figure S6A). In another case, stable HEK293T cell lines expressing the WT and mutants were developed to achieve more controlled protein expression, and the receptor-mediated apoptosis was evaluated in the form of a cell-viability measurement. Cell-surface expression levels were also similar among the DR5 variants according to anti-DR5 antibody immunostaining (Figure S5B). In both assays, the V227Y mutant, whose TMH assembly was not affected, showed the same signaling activity as the WT (Figures 5B and 5C). The estimated EC_{50} of TRAIL in these two experiments is 60–100 ng/mL. In contrast, single mutations that disrupt either dimeric (G217Y) or trimeric (T219Y, A222Y) interaction as well as the double mutation (G217Y and A222Y) that disrupts both interactions all abolished the receptor activity in these assays (Figures 5B and 5C). The TRAIL-induced signaling assays strongly indicated that both trimeric and dimeric interactions of the TMH are essential to DR5 signaling. While the need for TMH trimerization in receptor activation was expected from the study of Fas (Fu et al., 2016), the role of TMH dimerization is likely exerted by mediating higher-order receptor clustering, a concept that has not been previously attributed to the TMH.

A previous study showed that crosslinking TRAIL could greatly augment agonistic activity toward DR5 (Nair et al., 2015). This result led us to test whether crosslinking the TRAIL can compensate for the defect of the G217Y mutant to form higher-order clusters. For this experiment, we used TRAIL with N-terminal FLAG tag (FLAG-TRAIL) and anti-FLAG immunoglobulin G (IgG) to crosslink the TRAIL trimers. In this case, the antibody should provide the dimeric interactions that the G217Y mutant lacks. Indeed, for both transiently expressed G217Y mutant in DR5-deficient BJAB cells and stably expressed mutant in the stable HEK293T cells, crosslinking TRAIL with antibody rescued the inability of the mutant receptor to signal (Figures 5D and 5E), lending further support for the role of TMH dimerization in mediating higher-order receptor clustering.

To gather more direct evidences of TMH-mediated receptor clustering, we used confocal microscopy to examine

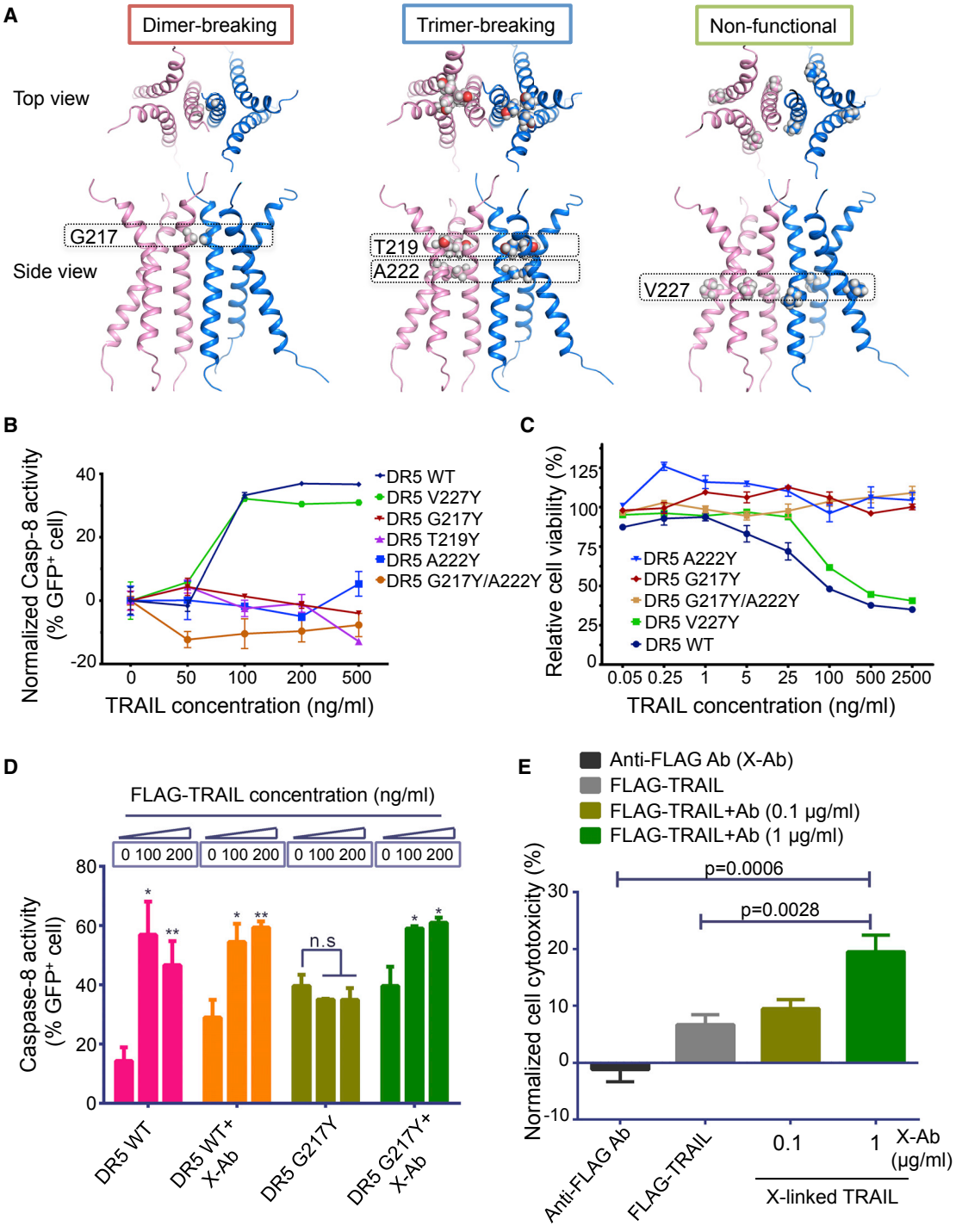

Figure 5. Essential Role of TMH Clustering in DR5 Signaling

(A) Positions of mutations in the DR5^{TMH} hexamer. Cartoon representation of the side and overviews of the dimer-of-trimers structure of DR5^{TMH} shows the positions of dimer-breaking mutation (G217Y), trimer-breaking mutations (T219Yand A222Y), and non-functional mutation (V227) (spheres) in the structure. The structure shows that V227 is not involved in either dimeric or trimeric interactions.

(B) TRAIL-induced apoptosis in DR5-deficient BJAB cells after transient transfection of the WT DR5 or mutants. After transient transfection, cells were treated with TRAIL for 5 h. Caspase-8 activity was measured using the CaspGLOW red caspase-8 activity kit and flow cytometry and calculated as the percentage of DsRed2^{+}/GFP^{+} cells relative to GFP^{+} cells (see Figure S5A). Results were obtained from 3 independent experiments (n = 3) and expressed as mean ± SEM.

(legend continued on next page)

ligand-induced DR5 clustering on the cell surface and the effect of TM mutations on cluster formation. In this experiment, the C terminus of DR5 was fused to the EGFP (designated DR5-EGFP). We transiently expressed DR5-EGFP, the corresponding tobacco etch virus (TEV)-cleavable version, and the dimer-breaking mutant (G217Y) separately in HEK293T cells and used confocal microscopy to examine their surface distribution before and after treatment with ligand or enzyme. As shown in Figure S6B, treating the cells expressing WT DR5-EGFP with TRAIL clearly resulted in the appearance of several very bright and elongated puncta on the cell surface, suggesting receptor clustering. As expected, treating the cells expressing TEV-cleavable DR5-EGFP with TEV enzyme also induced many bright puncta on the cell surface. However, treating the cells expressing the dimer-breaking mutant, while slightly increased fluorescence on the cell surface, did not generate any sharp bright puncta. Since the dimer-breaking mutation is in the TMH, the data suggest that the receptor clusters were mediated by TMH oligomerization.

TMH Higher-Order Clustering Alone Is Sufficient for DR5 Signaling, which Is Inhibited by the Unliganded ECD

The ability of $DR5^{TMH}$ alone to mediate a dimer-trimer network formation prompted us to wonder why full-length DR5 does not signal in the absence of ligand binding, and whether the ECD physically hinders TMH from clustering and activation of the signaling pathway (Figure 6A). To test this hypothesis, we inserted a TEV cleavage sequence (ENLYFQGGGGGS) at residue 208 between the ECD and TMH for proteolytic removal of ECD and appended the receptor C terminus with EGFP for facile separation of $DR5^{+}$ cells using flow cytometry analysis. The cleavable DR5 was transiently expressed in DR5-deficient BJAB cells. The modified receptor was still active as addition of TRAIL induced strong caspase-8 activity (Figure 6B). Remarkably, TEV protease treatment to remove the ECD activated DR5 in a dose-response manner (Figure 6C). The extent of caspase-8 activation mimicked ligand-induced activation (Figure 6B). Additionally, increase in receptor activity correlated with ECD removal from the cell surface, which was assessed by anti-DR5 antibodies (Figures S7A and S7B). In parallel, WT DR5 without the TEV cleavage site was not responsive to the protease except at a very high enzyme concentration (100 μg/mL) (Figure 6C). These results revealed that the pre-ligand state of ECD hinders the intrinsic ability of the TMH to assemble and activate the signaling pathway, and that the TMH, instead of the ECD, affords the driving force for assembly of the intracellular signaling complex.

Effect of TMH Oligomerization on the Pre-ligand Form of DR5

To further examine the role of the TMH in pre-ligand and ligand-dependent DR5 associations, we implemented a fluorescence resonance energy transfer (FRET) assay used previously for investigating self-association of Fas and other receptors in the TNFRSF (Chan et al., 2000; Lee et al., 2009; Siegel et al., 2000a). In this experiment, the intracellular region of DR5 was replaced with either cyan fluorescent protein (CFP) or yellow fluorescent protein (YFP). The fluorescent CFP- and YFP-fused WT DR5 constructs, or those harboring TMH mutations, were transiently co-expressed in HEK293T cells, and the FRET efficiency between CFP and YFP, which quantitates receptor association, were measured by acceptor photobleaching FRET (Chan et al., 2000). Before ligand stimulation, the FRET efficiencies of WT and the A222Y mutant that is defective for TMH trimerization did not show significant difference (Figures 6D and 6E). This is consistent with previous data on Fas that trimer-breaking mutations did not alter the Fas pre-ligand oligomerization (Fu et al., 2016). Upon ligand addition, the FRET efficiency of WT DR5 increased significantly (Figures 6D and 6E). Similarly, the G217Y mutant also showed a significant increase in FRET efficiency after TRAIL binding. However, for the A222Y mutant that is defective in TMH trimerization, the FRET increase upon ligand binding was not significant compared to the experimental uncertainty. Together these data seem to suggest DR5 TMH trimerization does not influence receptor pre-ligand association but is critical for ligand-induced receptor clustering.

Unliganded ECD Also Inhibits Receptor Activation for TNFR2 and OX40

We further investigated whether proteolytic removal of ECD can also activate TNFR2 or OX40, two other members of the TNFRSF. Since the TMHs of the two receptors, like that of DR5, are expected to cluster owing to the GXXXG motif (Figure 7A), removal of the ECD ought to free the TMHs, allowing them to cluster and activate downstream signaling. We inserted a TEV cleavage site between the ECD and TMH as was done for DR5 above and used a nuclear factor κB (NF-κB) luciferase reporter to read out receptor activation by the TEV protease in the absence of the native ligands. The results show that both TEV-cleavable TNFR2 and OX40 could be activated by the protease in a dose-dependent manner, whereas the WT receptors were not responsive (Figures 7B and 7C).

(C) TRAIL-induced apoptosis in DR5-expressing HEK293T stable cell lines. Monoclonal HEK293T stable cell lines expressing the WT DR5 or mutants were treated with TRAIL for 12 h. Cell viability was determined by a cell-count kit (CCK-8) through measurement of dehydrogenase activities in live cells. Results were from 4 duplicates (n = 4), repeated two times in independent experiments, and expressed as mean ± SD.

(D) Rescue of the dimerization-defective mutant (G217Y) with crosslinked TRAIL in the DR5-deficient BJAB cells. After transient expression of WT or G217Y DR5, cells were treated with two different concentrations of FLAG-TRAIL (100, 200 ng/mL), each in the absence and presence of 500 ng/mL anti-FLAG IgG (designated X-Ab) for 5 h. Caspase-8 activity was measured as in (B) except the data were not normalized. Results were obtained from 3 independent experiments (n = 3) and expressed as mean ± SEM. Data were analyzed by unpaired Student's test, $^{*}p < 0.05$ and $^{**}p < 0.005$.

(E) The same study as in (D) performed using the HEK293T stable cells. Monoclonal HEK293T stable cell line expressing DR5 WT or G217Y mutant was treated with FLAG-TRAIL (100 ng/mL) in the absence and presence of 0.1 and 1 μg/mL anti-FLAG IgG (X-Ab) for 12 h. Cell cytotoxicity (100% cell viability) was determined using a cell-counting kit-8 (CCK-8) as described in (C). Results were from 3 duplicates (n = 3) and expressed as mean ± SD.

See also Figures S5 and S6.

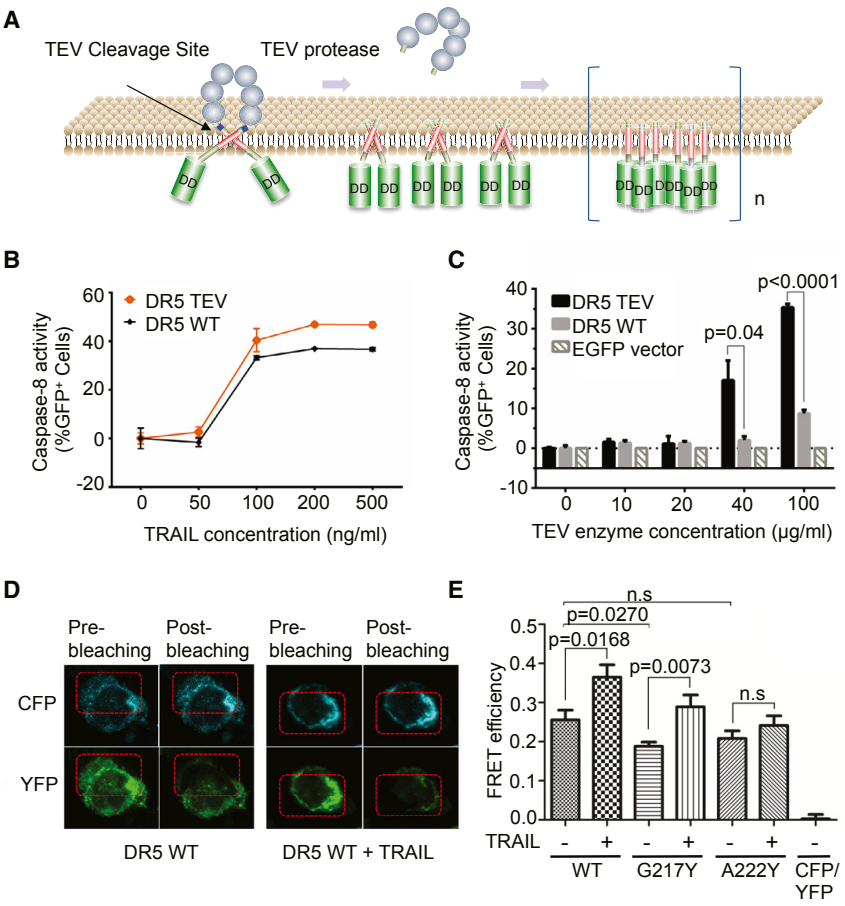

Figure 6. Higher-Order Clustering Is Inhibited by the Unliganded Extracellular Domain

(A) Schematic illustration of possible mechanism underlying proteolytic activation of DR5.

(B) Comparing TRAIL sensitivity of the DR5-TEV-expressing BJAB cells to that of the DR5-WT-expressing BJAB cells. Caspase-8 activity was measured using the CaspGLOW red caspase-8 activity kit (Biovision) and flow cytometry (BD FACSAria II) and was calculated as percentage of DsRed2$^+$/GFP$^+$ cells divided by percentage of GFP$^+$ cells. Results were from 3 independent experiments (n = 3) and expressed as mean ± SEM.

(C) TEV-induced apoptosis. DR5-deficient BJAB cells were transiently transfected with WT DR5-EGFP with (DR5-TEV) or without (DR5-WT) TEV cleavage site between the ECD and TMD. After transfection, BJAB cells were treated with TEV for 5 h before analysis.

(D) Examples of CFP and YFP photobleaching for WT DR5 without (left) and with (right) TRAIL.

(E) Receptor self-association of the WT DR5 and mutants. The effects of dimer-breaking mutation (G217Y) and trimer-breaking mutation (A222Y) with or without TRAIL pre-treatment are quantitated in the form of FRET efficiency. CFP/YFP co-transfected cells were used as FRET negative control. N.S., not significant. Twelve regions of interest (n = 12) (ROI; e.g., plasma membrane-bound DR5) from different cells were examined by FRET study.

See also Figures S6 and S7.

DISCUSSION

Intrinsic Dimer-Trimer Network of DR5 TMH Is Sufficient for Signaling, while a Role of the ECD Is Autoinhibition

In this study, we unexpectedly discovered that the single-pass TMH of DR5 has distinct trimerization and dimerization interfaces to allow the formation of higher-order structures in membrane, and that the TMH alone is sufficient to drive signaling in the absence of the ECD. While existing models of TNFRSF signaling rely on clustering by the ECD (Mukai et al., 2010; Valley et al., 2012; Vanamee and Faustman, 2018; Yang et al., 2005), our results in contrast revealed the necessary and sufficient role of the TMH in DR5 clustering and signaling. First, both TMH interfaces are necessary as structure-based single-point mutations in the TMH that disrupt either the trimeric or dimeric interaction abolished TRAIL-induced cell death. Second, the TMH-mediated dimer-trimer network is sufficient as we demonstrated full DR5 activation by proteolytic removal of the ECD, in the absence of ligand engagement.

In this context, we hypothesize that the primary consequence of ligand binding is to overcome the inhibitory restraint that the ECD places on the TMH by altering the pre-ligand conformation (Figure 7D). This autoinhibition hypothesis provides an explanation for the long-standing puzzle on how dimeric agonistic antibodies or the dimeric ligand NGF activate TNFRSF family members as trimeric TNF family ligands do, because many different ECD interactions may overcome a specific autoinhibition state, while ECD clustering with an optimal geometry to position the TMH is unlikely to achieve in the different dimer-trimer, trimer-trimer, or dimer-dimer networks that these different activating agents may assume with the receptors.

Disruption of the pre-ligand state by ligand binding is supported by the lack of crystal lattice-mediated dimeric associations of the unliganded TNFR1 ECD (Naismith et al., 1995) in the crystal structures of any ligand-receptor complexes in the TNFRSF (Vanamee and Faustman, 2018; Wu and Hymowitz, 2009). Additionally, mutations in the PLAD away from the ligand-binding site have been found to affect ligand binding, suggesting an allosteric coupling between ligand binding and PLAD association (Chan et al., 2000). There is also a tendency for agonistic antibodies to bind to the CRD1 and CRD2 regions of TNFRSF members that overlap with the ECD PLAD (Chodorge et al., 2012; Siegel et al., 2000b; Tamada et al., 2015), suggesting that breaking the PLAD interaction contributes to the agonistic phenotypes. Interestingly, O-linked glycosylation of DR5 ECD could augment ligand-induced receptor signaling (Wagner et al., 2007), which could also be explained by weakening of the PLAD interaction by O-Glycan modification

A

Protein	Transmembrane Sequence
DR5	..SLSGIIIGVTVAAVVLIVAV..
OX40	..LGLGLVLGLLGPLAILLALY..
TNFR2	..LPVGLIVGVTALGLLIIGVV..
DAP12	..VLAGIVMGDLVLTVLIALAV..

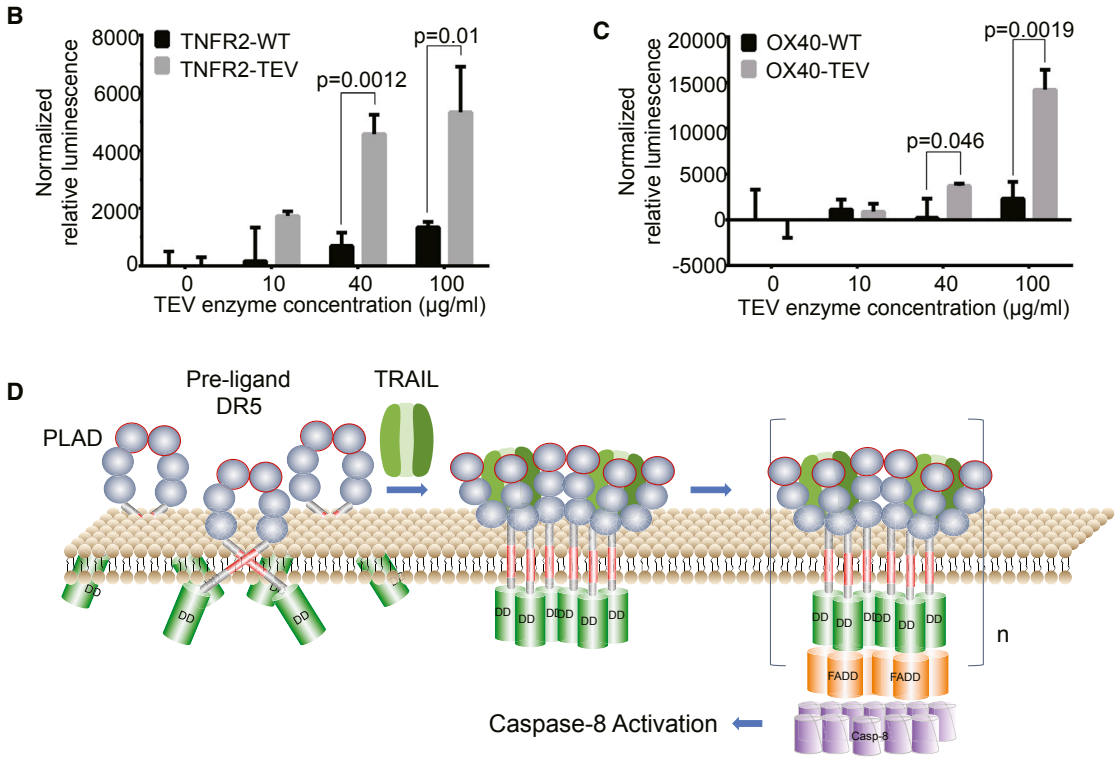

Figure 7. Proposed Roles of TMH in Ligand-Induced Receptor Assembly and Receptor Clustering

(A) Examples of other human receptor TMDs bearing the GXXXG motif that may mediate receptor clustering.

(B and C) Activation of TNFR2 (B) and OX40 (C) by proteolytic removal of the ECD in the absence of ligands. TEV cleavage site was inserted between the ECD and TMH for human TNFR2 and OX40. In 24-well plates, 20 μg of NF-κB plasmid and 50 μg of plasmid of the TEV-cleavable TNFR2/OX40 or the WT TNFR2/OX40 were co-transfected into HEK293T cells using Lipofectamine 3000 (Invitrogen). 14 h after transfection, cells were treated with 10, 40, or 100 μg/mL TEV enzyme for 5 h at 37°C. The cell lysates were analyzed for luminescence. Normalized relative luminescence is calculated as the difference between luminescence of the TEV-treated and non-TEV treated cell lysate divided by the cell lysate input (mg/mL). Results were from 3 independent experiments (n = 3) and expressed as mean ± SEM.

(D) A model of DR5 activation by TRAIL, highlighting how TRAIL binding to the ECD unleashes the TMH to trimerize and to form a higher-order cluster to activate downstream signaling.

of ECD. Collectively, our studies afford new opportunities and unique perspectives to modulate the signal transduction of these receptors for disease treatment including cancer immunotherapy.

The GXXXG Motif

The extraordinary function of a single TMH of DR5 to mediate both ligand-receptor complex assembly and higher-order receptor clustering may be attributed partly to the GXXXG motif. Previous studies of GXXXG-bearing receptor TMHs mainly reported the function of GXXXG in receptor assembly, e.g., EGFR (Endres et al., 2013) and ErbB2 (Bocharov et al., 2008). The current study uncovered an unrecognized function of GXXXG in receptor clustering. Notably, two other members of the TNFRSF, OX40 and TNFR2, also have TMHs that contain GXXXG, and they are expected to cluster similarly as that of DR5. Indeed, we found that both TNFR2 and OX40 could be efficiently activated by proteolytic removal of the receptor ECD in the absence of their respective ligands, suggesting that their TMHs drive downstream signaling in a manner similar to that of DR5. Furthermore, TMHs of some activating immunoreceptors such as the NKG2C-DAP12 complex also have conserved GXXXG motif, which is curiously not involved in receptor assembly (Call et al., 2010). Therefore, the role of GXXXG in mediating receptor clustering may represent a more general concept in receptor biology.

Possible Determinants of Receptor Cluster Formation

While the presence of distinct dimerization and trimerization interfaces on opposite faces of DR5 TMH implies the ability of the TMH to form large clusters as modeled in Figure 4D, our data are insufficient to address the cluster size *in vivo*. In the native setting, the TMH aggregation number could depend on obvious factors including geometrical constraints posed by the extra- and intra- cellular domains of the receptor, the local receptor concentration, as well as the biophysical properties of the relevant membrane. The clusters, however, do not have to be rigidly and uniformly structured arrays if their purpose is simply to concentrate laterally the intracellular signaling components to a level that the signaling-competent DISC can form. As such, the reversible dimeric and trimeric interactions among the TMHs could suffice to concentrate the full-length receptors on the cell surface and form large, dynamic clusters. Indeed, our confocal microscopy data that TRAIL could induce large puncta formation by the WT DR5 but not the G217Y mutant are consistent with the ability of TMH to mediate large-scale receptor clustering. Similar puncta have been observed previously for TNFR1 (Ko et al., 1999), Fas (Henkler et al., 2005), and 4-1BB (Gusti et al., 2014), although in those cases, factors other than the TMH could provide the dimeric interactions to achieve the dimer-trimer network.

STAR★METHODS

Detailed methods are provided in the online version of this paper and include the following:

- KEY RESOURCES TABLE
- CONTACT FOR REAGENT AND RESOURCE SHARING
- EXPERIMENTAL MODEL AND SUBJECT DETAILS
  - DR5-deficient BJAB cell line
  - HEK293T cell line
- METHOD DETAILS
  - Protein Expression and Purification
  - Reconstitution of $DR5^{TMH}$ in Bicelles
  - Analysis of the Oligomeric State of the WT and Mutant $DR5^{TMH}$ in Bicelles by SDS-PAGE and OG-Label
  - Assignment of NMR Resonances
  - Backbone Chemical Shift and TALOS Analyses
  - Assignment of NOE Restraints
  - Structure Calculation
  - Analysis of Transmembrane Partition of the Trimeric Mutant of $DR5^{TMH}$
  - TRAIL Preparation
  - Ligand-Induced DR5 Activation Assay Using DR5-Expressing Stable Cell Line
  - Cell Imaging
  - Ligand-Induced DR5 Activation Assay Using Transiently Transfected Cells
  - Fluorescence Resonance Energy Transfer
  - Apoptosis Induced by TEV Cleavage-Mediated DR5 ECD Removal
  - TEV Cleavage Validation by Flow Cytometry
- QUANTIFICATION AND STATISTICAL ANALYSIS
- DATA AND SOFTWARE AVAILABILITY

SUPPLEMENTAL INFORMATION

Supplemental Information can be found with this article online at https://doi.org/10.1016/j.cell.2019.02.001.

ACKNOWLEDGMENTS

This work was supported by the National Key Research and Development Program of China (2017YFC0908600) and the National Natural Science Foundation of China (81430081) (to S.C.), NIH grant GM116898 (to J.J.C.), and NIH grants 1DP1 HD087988 and AI050872 (to H.W.). The NMR data were collected at the NMR facility of NCPSS (supported by CAS grant XDB08030301) and MIT-Harvard CMR (supported by NIH grant P41 EB-002026).

AUTHOR CONTRIBUTIONS

L.P., T.-M.F., S.C., H.W., and J.J.C. conceived of the study. L.P., L.Z., and Q.F. prepared samples for NMR and *in vitro* assembly studies. W.C. performed the OG-label assay. L.P., L.Z., Q.F., Z.L., and J.J.C. collected and analyzed NMR data and/or determined the structures. A.P., L.Z., and L.P. performed membrane partition analysis. T.-M.F., W.Z., L.P., C.Q., S.C., H.W., and J.J.C. performed and/or analyzed functional experiments. J.J.C., H.W., and L.P. wrote the paper, and all authors contributed to editing of the manuscript.

DECLARATION OF INTERESTS

The authors declare no competing interests.

Received: July 9, 2018
Revised: November 14, 2018
Accepted: January 29, 2019
Published: February 28, 2019

REFERENCES

Ashkenazi, A. (2008). Targeting the extrinsic apoptosis pathway in cancer. Cytokine Growth Factor Rev. *19*, 325–331.

Ashkenazi, A., and Dixit, V.M. (1998). Death receptors: signaling and modulation. Science *281*, 1305–1308.

Ashkenazi, A., Pai, R.C., Fong, S., Leung, S., Lawrence, D.A., Marsters, S.A., Blackie, C., Chang, L., McMurtrey, A.E., Hebert, A., et al. (1999). Safety and antitumor activity of recombinant soluble Apo2 ligand. J. Clin. Invest. *104*, 155–162.

Baker, S.J., and Reddy, E.P. (1998). Modulation of life and death by the TNF receptor superfamily. Oncogene *17*, 3261–3270.

Bartels, C., Xia, T.H., Billeter, M., Güntert, P., and Wüthrich, K. (1995). The program XEASY for computer-supported NMR spectral analysis of biological macromolecules. J. Biomol. NMR *6*, 1–10.

Bocharov, E.V., Mineev, K.S., Volynsky, P.E., Ermolyuk, Y.S., Tkach, E.N., Sobol, A.G., Chupin, V.V., Kirpichnikov, M.P., Efremov, R.G., and Arseniev, A.S. (2008). Spatial structure of the dimeric transmembrane domain of the growth factor receptor ErbB2 presumably corresponding to the receptor active state. J. Biol. Chem. *283*, 6950–6956.

Boldin, M.P., Mett, I.L., Varfolomeev, E.E., Chumakov, I., Shemer-Avni, Y., Camonis, J.H., and Wallach, D. (1995). Self-association of the "death domains" of the p55 tumor necrosis factor (TNF) receptor and Fas/APO1 prompts signaling for TNF and Fas/APO1 effects. J. Biol. Chem. *270*, 387–391.

Call, M.E., Wucherpfennig, K.W., and Chou, J.J. (2010). The structural basis for intramembrane assembly of an activating immunoreceptor complex. Nat. Immunol. *11*, 1023–1029.

Chan, F.K. (2007). Three is better than one: pre-ligand receptor assembly in the regulation of TNF receptor signaling. Cytokine *37*, 101–107.

Chan, F.K., Chun, H.J., Zheng, L., Siegel, R.M., Bui, K.L., and Lenardo, M.J. (2000). A domain in TNF receptors that mediates ligand-independent receptor assembly and signaling. Science *288*, 2351–2354.

Chaudhary, P.M., Eby, M., Jasmin, A., Bookwalter, A., Murray, J., and Hood, L. (1997). Death receptor 5, a new member of the TNFR family, and DR4 induce FADD-dependent apoptosis and activate the NF-kappaB pathway. Immunity *7*, 821–830.

Chen, W., Dev, J., Mezhyrova, J., Pan, L., Piai, A., and Chou, J.J. (2018). The Unusual Transmembrane Partition of the Hexameric Channel of the Hepatitis C Virus. Structure *26*, 627–634.

Chodorge, M., Züger, S., Stirnimann, C., Briand, C., Jermutus, L., Grütter, M.G., and Minter, R.R. (2012). A series of Fas receptor agonist antibodies that demonstrate an inverse correlation between affinity and potency. Cell Death Differ. *19*, 1187–1195.

Cooper, D., Bansal-Pakala, P., and Croft, M. (2002). 4-1BB (CD137) controls the clonal expansion and survival of CD8 T cells in vivo but does not contribute to the development of cytotoxicity. Eur. J. Immunol. *32*, 521–529.

Delaglio, F., Grzesiek, S., Vuister, G.W., Zhu, G., Pfeifer, J., and Bax, A. (1995). NMRPipe: a multidimensional spectral processing system based on UNIX pipes. J. Biomol. NMR *6*, 277–293.

Driscoll, P.C. (2014). Structural studies of death receptors. Methods Enzymol. *545*, 201–242.

Endres, N.F., Das, R., Smith, A.W., Arkhipov, A., Kovacs, E., Huang, Y., Pelton, J.G., Shan, Y., Shaw, D.E., Wemmer, D.E., et al. (2013). Conformational coupling across the plasma membrane in activation of the EGF receptor. Cell *152*, 543–556.

Esposito, D., Sankar, A., Morgner, N., Robinson, C.V., Rittinger, K., and Driscoll, P.C. (2010). Solution NMR investigation of the CD95/FADD homotypic death domain complex suggests lack of engagement of the CD95 C terminus. Structure *18*, 1378–1390.

Fu, Q., Fu, T.M., Cruz, A.C., Sengupta, P., Thomas, S.K., Wang, S., Siegel, R.M., Wu, H., and Chou, J.J. (2016). Structural Basis and Functional Role of Intramembrane Trimerization of the Fas/CD95 Death Receptor. Mol. Cell *61*, 602–613.

Glover, K.J., Whiles, J.A., Wu, G., Yu, N., Deems, R., Struppe, J.O., Stark, R.E., Komives, E.A., and Vold, R.R. (2001). Structural evaluation of phospholipid bicelles for solution-state studies of membrane-associated biomolecules. Biophys. J. *81*, 2163–2171.

Grønbaek, K., Straten, P.T., Ralfkiaer, E., Ahrenkiel, V., Andersen, M.K., Hansen, N.E., Zeuthen, J., Hou-Jensen, K., and Guldberg, P. (1998). Somatic Fas mutations in non-Hodgkin's lymphoma: association with extranodal disease and autoimmunity. Blood *92*, 3018–3024.

Gusti, V., Bennett, K.M., and Lo, D.D. (2014). CD137 signaling enhances tight junction resistance in intestinal epithelial cells. Physiol. Rep. *2*. Published online August 5, 2014. https://doi.org/10.14814/phy2.12090.

Hatzoglou, A., Roussel, J., Bourgeade, M.F., Rogier, E., Madry, C., Inoue, J., Devergne, O., and Tsapis, A. (2000). TNF receptor family member BCMA (B cell maturation) associates with TNF receptor-associated factor (TRAF) 1, TRAF2, and TRAF3 and activates NF-kappa B, elk-1, c-Jun N-terminal kinase, and p38 mitogen-activated protein kinase. J. Immunol. *165*, 1322–1330.

Henkler, F., Behrle, E., Dennehy, K.M., Wicovsky, A., Peters, N., Warnke, C., Pfizenmaier, K., and Wajant, H. (2005). The extracellular domains of FasL and Fas are sufficient for the formation of supramolecular FasL-Fas clusters of high stability. J. Cell Biol. *168*, 1087–1098.

Ko, Y.G., Lee, J.S., Kang, Y.S., Ahn, J.H., and Seo, J.S. (1999). TNF-alpha-mediated apoptosis is initiated in caveolae-like domains. J. Immunol. *162*, 7217–7223.

Lata, S., Reichel, A., Brock, R., Tampé, R., and Piehler, J. (2005). High-affinity adaptors for switchable recognition of histidine-tagged proteins. J. Am. Chem. Soc. *127*, 10205–10215.

Lee, S.H., Shin, M.S., Kim, H.S., Park, W.S., Kim, S.Y., Jang, J.J., Rhim, K.J., Jang, J., Lee, H.K., Park, J.Y., et al. (2000). Somatic mutations of Fas (Apo-1/CD95) gene in cutaneous squamous cell carcinoma arising from a burn scar. J. Invest. Dermatol. *114*, 122–126.

Lee, J.J., Rauter, I., Garibyan, L., Ozcan, E., Sannikova, T., Dillon, S.R., Cruz, A.C., Siegel, R.M., Bram, R., Jabara, H., et al. (2009). The murine equivalent of the A181E TACI mutation associated with CVID severely impairs B cell function. Blood *114*, 2254–2262.

MacKenzie, K.R., Prestegard, J.H., and Engelman, D.M. (1997). A transmembrane helix dimer: structure and implications. Science *276*, 131–133.

Mukai, Y., Nakamura, T., Yoshikawa, M., Yoshioka, Y., Tsunoda, S., Nakagawa, S., Yamagata, Y., and Tsutsumi, Y. (2010). Solution of the structure of the TNF-TNFR2 complex. Sci. Signal. *3*, ra83.

Nagata, S., and Golstein, P. (1995). The Fas death factor. Science *267*, 1449–1456.

Nair, P.M., Flores, H., Gogineni, A., Marsters, S., Lawrence, D.A., Kelley, R.F., Ngu, H., Sagolla, M., Komuves, L., Bourgon, R., et al. (2015). Enhancing the antitumor efficacy of a cell-surface death ligand by covalent membrane display. Proc. Natl. Acad. Sci. USA *112*, 5679–5684.

Naismith, J.H., Devine, T.Q., Brandhuber, B.J., and Sprang, S.R. (1995). Crystallographic evidence for dimerization of unliganded tumor necrosis factor receptor. J. Biol. Chem. *270*, 13303–13307.

Piai, A., Dev, J., Fu, Q., and Chou, J.J. (2017a). Stability and Water Accessibility of the Trimeric Membrane Anchors of the HIV-1 Envelope Spikes. J. Am. Chem. Soc. *139*, 18432–18435.

Piai, A., Fu, Q., Dev, J., and Chou, J.J. (2017b). Optimal Bicelle Size q for Solution NMR Studies of the Protein Transmembrane Partition. Chemistry *23*, 1361–1367.

Rieux-Laucat, F., Le Deist, F., Hivroz, C., Roberts, I.A., Debatin, K.M., Fischer, A., and de Villartay, J.P. (1995). Mutations in Fas associated with human lymphoproliferative syndrome and autoimmunity. Science *268*, 1347–1349.

Rogers, P.R., Song, J., Gramaglia, I., Killeen, N., and Croft, M. (2001). OX40 promotes Bcl-xL and Bcl-2 expression and is essential for long-term survival of CD4 T cells. Immunity *15*, 445–455.

Salzmann, M., Wider, G., Pervushin, K., and Wüthrich, K. (1999). Improved sensitivity and coherence selection for [15N,1H]-TROSY elements in triple resonance experiments. J. Biomol. NMR *15*, 181–184.

Sanders, C.R., Hare, B.J., Howard, K.P., and Prestegard, J.H. (1994). Magnetically-Oriented Phospholipid Micelles As A Tool For The Study Of Membrane-Associated Molecules. Prog. Nucl. Magn. Reson. Spectrosc. *26*, 421–444.

Schwieters, C.D., Kuszewski, J.J., Tjandra, N., and Clore, G.M. (2003). The Xplor-NIH NMR molecular structure determination package. J. Magn. Reson *160*, 65–73.

Shen, Y., Delaglio, F., Cornilescu, G., and Bax, A. (2009). TALOS+: a hybrid method for predicting protein backbone torsion angles from NMR chemical shifts. J. Biomol. NMR *44*, 213–223.

Sheridan, J.P., Marsters, S.A., Pitti, R.M., Gurney, A., Skubatch, M., Baldwin, D., Ramakrishnan, L., Gray, C.L., Baker, K., Wood, W.I., et al. (1997). Control of TRAIL-induced apoptosis by a family of signaling and decoy receptors. Science *277*, 818–821.

Siegel, R.M., Chan, F.K., Zacharias, D.A., Swofford, R., Holmes, K.L., Tsien, R.Y., and Lenardo, M.J. (2000a). Measurement of molecular interactions in living cells by fluorescence resonance energy transfer between variants of the green fluorescent protein. Sci. STKE *2000*, pl1.

Siegel, R.M., Frederiksen, J.K., Zacharias, D.A., Chan, F.K., Johnson, M., Lynch, D., Tsien, R.Y., and Lenardo, M.J. (2000b). Fas preassociation required for apoptosis signaling and dominant inhibition by pathogenic mutations. Science *288*, 2354–2357.

Szyperski, T., Neri, D., Leiting, B., Otting, G., and Wüthrich, K. (1992). Support of 1H NMR assignments in proteins by biosynthetically directed fractional 13C-labeling. J. Biomol. NMR *2*, 323–334.

Tamada, T., Shinmi, D., Ikeda, M., Yonezawa, Y., Kataoka, S., Kuroki, R., Mori, E., and Motoki, K. (2015). TRAIL-R2 Superoligomerization Induced by Human Monoclonal Agonistic Antibody KMTR2. Sci. Rep. *5*, 17936.

Trenker, R., Call, M.E., and Call, M.J. (2015). Crystal Structure of the Glycophorin A Transmembrane Dimer in Lipidic Cubic Phase. J. Am. Chem. Soc. *137*, 15676–15679.

Valley, C.C., Lewis, A.K., Mudaliar, D.J., Perlmutter, J.D., Braun, A.R., Karim, C.B., Thomas, D.D., Brody, J.R., and Sachs, J.N. (2012). Tumor necrosis factor-related apoptosis-inducing ligand (TRAIL) induces death receptor 5 networks that are highly organized. J. Biol. Chem. *287*, 21265–21278.

Vanamee, E.S., and Faustman, D.L. (2018). Structural principles of tumor necrosis factor superfamily signaling. Sci. Signal. *11*. Published online January 2, 2018. https://doi.org/10.1126/scisignal.aao4910.

Vranken, W.F., Boucher, W., Stevens, T.J., Fogh, R.H., Pajon, A., Llinas, M., Ulrich, E.L., Markley, J.L., Ionides, J., and Laue, E.D. (2005). The CCPN data model for NMR spectroscopy: development of a software pipeline. Proteins *59*, 687–696.

Wagner, K.W., Punnoose, E.A., Januario, T., Lawrence, D.A., Pitti, R.M., Lancaster, K., Lee, D., von Goetz, M., Yee, S.F., Totpal, K., et al. (2007). Death-receptor O-glycosylation controls tumor-cell sensitivity to the proapoptotic ligand Apo2L/TRAIL. Nat. Med. *13*, 1070–1077.

Wajant, H. (2002). The Fas signaling pathway: more than a paradigm. Science *296*, 1635–1636.

Wang, L., Yang, J.K., Kabaleeswaran, V., Rice, A.J., Cruz, A.C., Park, A.Y., Yin, Q., Damko, E., Jang, S.B., Raunser, S., et al. (2010). The Fas-FADD death domain complex structure reveals the basis of DISC assembly and disease mutations. Nat. Struct. Mol. Biol. *17*, 1324–1329.

Watts, T.H. (2005). TNF/TNFR family members in costimulation of T cell responses. Annu. Rev. Immunol. *23*, 23–68.

Wu, H., and Hymowitz, S.G. (2009). Structure and function of tumor necrosis factor (TNF) at the cell surface. In Handbook of Cell Signaling, R.A. Bradshaw and E.A. Dennis, eds. (Academic Press), pp. 265–275.

Wu, H., Su, K., Guan, X., Sublette, M.E., and Stark, R.E. (2010). Assessing the size, stability, and utility of isotropically tumbling bicelle systems for structural biology. Biochim. Biophys. Acta *1798*, 482–488.

Yang, J.K., Wang, L., Zheng, L., Wan, F., Ahmed, M., Lenardo, M.J., and Wu, H. (2005). Crystal structure of MC159 reveals molecular mechanism of DISC assembly and FLIP inhibition. Mol. Cell *20*, 939–949.

Yang, J., Piai, A., Shen, H.B., and Chou, J.J. (2017). An Exhaustive Search Algorithm to Aid NMR-Based Structure Determination of Rotationally Symmetric Transmembrane Oligomers. Sci. Rep. *7*, 17373.

STAR★METHODS

KEY RESOURCES TABLE

REAGENT or RESOURCE	SOURCE	IDENTIFIER
Antibodies		
Anti-DR5 mAbs-FITC	Abcam	Cat# ab53319; RRID:AB_2204941
Anti-FLAG mAbs, M2	Sigma-Aldrich	Cat# F1804; RRID:AB_262044
Primary anti-DR5 mAbs	R&D systems	Cat# mab631; RID:AB_2204811
Goat Anti-Mouse IgG H&L (Alexa Fluor 647)	Abcam	Cat# ab150115; RRID:AB_2687948
Bacterial Strains and mammalian cells		
E. coli BL21(DE3)	New England Biolabs	Cat# C2527
E. coli DH5-alpha	New England Biolabs	Cat# C2987
HEK293T	ATCC	CRL-3216; RRID:CVCL_0063
DR5-deficient BJAB cell	Andrew Thorburn	N/A
Chemicals, Peptides, and Recombinant Proteins		
Cyanogen Bromide	Sigma-Aldrich	Cat# C91492
Isotopes	Cambridge Isotope Laboratories	N/A
Kanamycin monosulfate	Sigma-Aldrich	Cat# BP861
Ampicillin, Sodium Salt	Sigma-Aldrich	Cat# 171254
Puromycin dihydrochloride	Sigma-Aldrich	Cat# P8833
isopropyl β-D-thiogalatopyranoside (IPTG)	Sigma-Aldrich	Cat# I5502
Imidazole	Sigma-Aldrich	Cat# I5513
Ammonium sulfate	Sigma-Aldrich	Cat# A4418
DTSSP (3,3′-dithiobis (sulfosuccinimidyl propionate))	ThermoFisher Scientific	Cat# 21578
Sulfo-NHS Acetate	Thermo Scientific	Cat# 26777
DMPC Lipid	Avanti Polar Lipids	Cat# 850345
DH^6PC Detergent	Avanti Polar Lipids	Cat# 850305
Deuterated DMPC lipid	Avanti Polar Lipids	Cat# 860345C
Deuterated DH^6PC Detergent	Avanti Polar Lipids	Cat# 790427C
TriNTA	Medicilon	N/A
SMCC Crosslinker	Life Technology	Cat# 22103
Triethylammonium Acetate	Calbiochem	Cat# 625718
Gd-DOTA	Macrocyclics	Cat# M-147
16-DSA	Sigma-Aldrich	Cat# 253596
$TRAIL_{114-281}$	This paper	N/A
FLAG-TRAIL	Enzo Life Sciences	Cat# ALX-522-003-C010
TEV enzyme	James Chou lab	N/A
Software and Algorithms		
Sparky	Goddard, UCSF	www.cgl.ucsf.edu/home/sparky
Nmrpipe	Delaglio et al., 1995	https://www.ibbr.umd.edu/nmrpipe
Ccpnmr	Vranken et al., 2005	http://www.ccpn.ac.uk
Origin	OriginLab	https://www.originlab.com/
Pymol	Schrodinger	https://pymol.org/2/
Talos+	Shen et al., 2009	https://www.ibbr.umd.edu/nmrpipe
Graphpad prism 6.01	Graphpad	https://www.graphpad.com/scientific-software/prism/

(*Continued on next page*)

Continued

REAGENT or RESOURCE	SOURCE	IDENTIFIER
Vectors and plasmids		
pVRC8400-puro	Tim Springer lab	N/A
pVRC-DR5 WT, for stable cell line	This paper	N/A
pVRC-DR5 G217Y, for stable cell line	This paper	N/A
pVRC-DR5 T219Y, for stable cell line	This paper	N/A
pVRC-DR5 A222Y, for stable cell line	This paper	N/A
pVRC-DR5 G217Y and A222Y, for stable cell line	This paper	N/A
pVRC-DR5 A227Y, for stable cell line	This paper	N/A
pEYFP-N1 vector	Clontech	Cat# 6006-1
pECFP-N1 vector	Clontech	Cat# 6900-1
pEYFP-N1-DR5 WT ΔCT	This paper	N/A
pECFP-N1-DR5 WT ΔCT	This paper	N/A
pEYFP-N1-DR5 G217Y ΔCT	This paper	N/A
pECFP-N1-DR5 G217Y ΔCT	This paper	N/A
pEYFP-N1-DR5 A222Y ΔCT	This paper	N/A
pECFP-N1-DR5 A222Y ΔCT	This paper	N/A
pMM-LR6 vector	Stephen C. Blacklow	N/A
pMM-DR5$_{TM}$ WT	This paper	N/A
pMM-DR5$_{TM}$ G217Y	This paper	N/A
pMM-DR5$_{TM}$ T219Y	This paper	N/A
pMM-DR5$_{TM}$ A222Y	This paper	N/A
pMM-DR5$_{TM}$ WT-6HIS, for OG-Label	This paper	N/A
pMM-DR5$_{TM}$ G217Y-6HIS, for OG-Label	This paper	N/A
pMM-DR5$_{TM}$ A227Y-6HIS, for OG-Label	This paper	N/A
pcDNA3-GFP-LIC vector	Scott Gradia	Addgene plasmid # 30127
pcDNA3-GFP-DR5 WT	This paper	N/A
pcDNA3-GFP-DR5 G217Y	This paper	N/A
pcDNA3-GFP-DR5 T219Y	This paper	N/A
pcDNA3-GFP-DR5 A222Y	This paper	N/A
pcDNA3-GFP-DR5 G217Y and A222Y	This paper	N/A
pcDNA3-GFP-DR5 V227Y	This paper	N/A
pcDNA3-GFP-DR5 TEV	This paper	N/A
pHAGE-NF-kappa B	Darrell Kotton	Addgene plasmid # 49343
pcDNA3.1(+)-OX40	Genscript	N/A
pcDNA3.1(+)-TNFR2	Genscript	N/A
pET28a(+)-TRAIL$_{114-281}$	Genscript	N/A
Other		
Hispur Ni-NTA Resin	ThermoFisher Scientific	Cat# 88223
Zorbax SB-C18 Column	Agilent	Cat# 880995-202
Centricon Concentrator	EMD Millipore	Cat# UFC901024
StrepTrap HP Column	GE Healthcare	Cat# 28907547
Superdex S75 26/60	GE Healthcare	Cat# 28989334
NHS-Activated Agrose Resin	Thermo Fisher	Cat# 26196
Hitrap phenyl FF column	GE Healthcare	Cat # 45-000-249
PD-10 column	GE Healthcare	Cat # 17085101
CaspGLOW Red Active Caspase-8 Staining Kit	BioVision	Cat # K198
Cell Counting Kit-8	Dojindo	Cat # CK04

(*Continued on next page*)

Continued

REAGENT or RESOURCE	SOURCE	IDENTIFIER
Hoechst 33342 Solution	ThermoFisher Scientific	Cat # 62249
Lipofectamine 2000 Transfection Reagent	ThermoFisher Scientific	Cat # 11668019
Lipofectamine 3000 Transfection Reagent	ThermoFisher Scientific	Cat # L3000008
Cell Line Nucleofector Kit V	Lonza	Cat# VVCA-1003
Dual Luciferase Reporter Assay kit	Promega	Cat# E1910
NuPAGE 10% Bis-Tris Protein Gels	ThermoFisher Scientific	Cat# NP0302BOX
NuPAGE 4-12% Bis-Tris Protein Gels	ThermoFisher Scientific	Cat# NP0322BOX

CONTACT FOR REAGENT AND RESOURCE SHARING

Further information and requests for resources and reagents should be directed to and will be fulfilled by the Lead Contact, James J. Chou (james_chou@hms.harvard.edu).

EXPERIMENTAL MODEL AND SUBJECT DETAILS

DR5-deficient BJAB cell line

Human Burkitt lymphoma B cell line -DR5-deficient BJAB was maintained in RPMI 1640 (GIBCO, ThermoFisher Scientific) plus 10% fetal bovine serum (GIBCO, ThermoFisher Scientific), and 100U/ml Pen-Strep (GIBCO, ThermoFisher Scientific), at 37°C, 5% CO_2.

HEK293T cell line

Human kidney epithelial cell line HEK293T and related DR5-expressing stable cell lines were maintained in DMEM (GIBCO, ThermoFisher Scientific) plus 10% fetal bovine serum (GIBCO, ThermoFisher Scientific), and 100U/ml Pen-Strep (GIBCO, ThermoFisher Scientific), at 37°C, 5% CO_2.

METHOD DETAILS

Protein Expression and Purification

The human DR5 (isoform 1) fragment, residues 208 – 242, corresponding to the TMH was synthesized by GenScript (Piscataway, NJ) (Figure S1A). Amino acid C209 within stalk region was mutated to glycine, as DR5S (short form) with no stalk region is functional as DR5L (long form). This fragment is designated $DR5^{TMH}$. Expression constructs were created by fusing the $DR5^{TMH}$ fragment to the C terminus of the His9-TrpLE expression sequence in pMM-LR6 vector (a gift from S.C. Blacklow, Harvard Medical School), with an added methionine in-between for cleavage by cyanogen bromide. Mutant constructs were generated by standard PCR protocols and confirmed by DNA sequencing. For NMR sample preparation, transformed *E. coli* strain BL21 (DE3) cells were grown in M9 minimal media supplemented with Centrum multivitamins and stable isotopes. Cultures were grown at 37°C to an absorbance of ~0.6 at 600 nm, and cooled to 28°C before induction with 600 μM isopropyl β-D-thiogalatopyranoside at 28°C for overnight. For fully deuterated proteins, bacterial cultures were grown in 99.8% D_2O (Sigma Aldrich, St. Louis, MO) with deuterated glucose (Cambridge Isotope Laboratories, Tewksbury, MA). The $DR5^{TMH}$ protein was extracted, cleaved by cyanogen bromide, purified and lyophilized as described (Fu et al., 2016). Some of the differences are stated below. To keep Cys232 reduced, 20 mM BME (2-Mercaptoethanol) was used throughout the Ni-NTA purification step. Because $DR5^{TMH}$ is very hydrophobic, it was still bound to the column after the elution gradient from 50% (v/v) isopropanol with 0.1% (v/v) trifluoroacetic acid (Buffer A) to 100% (v/v) acetonitrile with 5% (v/v) isopropanol and 0.1% (v/v) trifluoroacetic acid (Buffer B) (Figure S1B). A second elution gradient from 0% to 100% Buffer B was needed to elute $DR5^{TMH}$ (Figure S1B).

Reconstitution of $DR5^{TMH}$ in Bicelles

To reconstitute the $DR5^{TMH}$ variants in bicelles, 1~2 mg of purified and lyophilized protein was mixed with 9 mg 1,2-Dimyristoyl-*sn*-Glycero-3-Phosphocholine (DMPC; protonated or deuterated from Avanti Ploar Lipids, Alabaster, AL) and dissolved in hexafluoro-isopropanol. The mixture was slowly dried to a thin film under nitrogen stream, followed by overnight lyophilization. The dried thin film was redissolved in 3 mL of 8 M Urea containing ~27 mg 1,2-Dihexanoyl-*sn*-Glycero-3-Phosphocholine (DHPC, D6PC; protonated or deuterated from Avanti Polar Lipids) and 20 mM 2-Mercaptoethanol (BME). The mixture was dialyzed twice against a 20 mM phosphate buffer (pH 7) (1 L each time) to remove the denaturant, and 10 mg D6PC was added to the sample before the second dialysis to compensate its loss. The DMPC:DHPC ratio was monitored by 1D NMR throughout the reconstitution process. If needed, additional D6PC was added to make the final DMPC:DHPC ratio between 0.5 and 0.6 (Figure S1C). The sample was concentrated using Centricon (EMD Millipore, Billerica, MA) to ~350 μl. The final NMR sample contained ~0.8 mM $DR5^{TMH}$ (monomer), ~50 mM DMPC,

~100 mM DHPC, 20 mM phosphate buffer (pH 7), 0.02% NaN_3 and 5% D_2O. For all NOE experiments, the protein was reconstituted using DMPC and DHPC with deuterated acyl chains (Avanti Polar Lipids).

Analysis of the Oligomeric State of the WT and Mutant DR5^{TMH} in Bicelles by SDS-PAGE and OG-Label

Standard SDS-PAGE was first used to examine the oligomeric state of the bicelle-reconstituted DR5^{TMH}. The WT or mutant DR5^{TMH} was reconstituted in bicelles (q ~0.5), and then mixed with a SDS sample buffer (Invitrogen) without boiling, followed by SDS-PAGE at 200 V for 30 minutes and Commassie blue staining. In the cases of the WT DR5^{TMH} and the G217Y and V227Y mutants, the unreconstituted protein migrated at apparent MW of ~5 kDa (theoretical MW of DR5^{TMH} is 3.6 kDa), and the bicelle-reconstituted protein migrated at ~16 kDa, which corresponds to a trimer. Although the trimeric interaction of DR5^{TMH} resisted SDS, the dimeric interaction did not. Therefore, the oligomeric state was further examined using the non-denaturing method known as OG-label.

In the OG-label method, each of the protomers in the membrane protein oligomer was labeled, non-covalently, with a soluble crosslinkable protein (SCP) protein. Then the SCPs were crosslinked with Lomant's reagents to read out the oligomeric state (schematically illustrated in Figure 2E). The SCP used was a small Ig-fold protein named GB1 (MW = 8.4 kDa), and its N terminus was linked to a TriNTA molecule via a PEG-2-SMCC ((succinimidyl 4-(N-maleimidomethyl) cyclohexane-1-carboxylate)) to form the TriNTA-GB1 conjugate as previously described (Chen et al., 2018). The membrane protein to be examined has a His_6-tag. TriNTA has high binding affinity to His_6-tag (20 ± 10 nM) (Lata et al., 2005), which can strongly attach GB1 to the individual protomers of the membrane protein oligomer in bicelles. Then, the concentration of stoichiometric number of GB1 to the membrane protein oligomer allows for more efficient crosslinking than the free GB1 in solution. The crosslinked GB1 can be released from the oligomer by addition of EDTA and analyzed by SDS-PAGE.

To implement the OG-label method for DR5^{TMH}, the protein was modified by a C terminus addition of a His_6-tag. The His_6-tagged DR5^{TMH} was expressed, purified, and reconstituted in bicelles (q ~0.5) in the same way as described above for other NMR samples except HEPES (pH 7.2) was used as buffer for better crosslinking efficiency. To prevent undesirable crosslinking between DR5^{TMH} and GB1, we first blocked all the active amine groups with the addition of 100-fold molar excess of Sulfo-NHS Acetate (Thermo Fisher Scientific) to the bicelle sample in 25 mM HEPES buffer (pH 7.2) for 1 hour at room temperature. Excessive Sulfo-NHS Acetate was removed by dialysis while tightly controlling the bicelle q. After dialysis, 20 μM DR5^{TMH} (monomer concentration) was mixed with 30 μM TriNTA-GB1 to ensure the His_6-tagged DR5^{TMH} are saturated with TriNTA-GB1. The mixture was then treated with 0.6 mM of DTSSP for 30 min, followed by incubation with various concentration (0.1, 0.5, 1.0, and 2.5 mM) of glutaraldehyde for 5 min. The crosslinking reaction was quenched with a 20 mM Tris buffer (pH 7.5). As a negative control, 0.6 mM of DTSSP and 0.5 mM of glutaraldehyde were sequentially added to 30 μM TriNTA-GB1 in the absence of the His_6-tagged DR5^{TMH}. The crosslinked species were boiled and examined by SDS-PAGE using the 4%–12% Bis-Tris protein gels (Thermo Fisher Scientific).

Assignment of NMR Resonances

All NMR data was collected at 30°C (303k) on Bruker spectrometers operating at ^1H frequency of 900 MHz, 800 MHz, 750 MHz, or 600 MHz and equipped with cryogenic probes. NMR data was processed using NMRPipe (Delaglio et al., 1995) and spectra analysis was performed in NMRPipe (Delaglio et al., 1995), Sparky (T. D. Goddard and D. G. Kneller, SPARKY 3, University of California, San Francisco), and XEASY (Bartels et al., 1995). Sequence specific assignment of backbone chemical shifts was accomplished using two pairs of TROSY-enhanced triple resonance experiments (Salzmann et al., 1999), recorded using a (^{15}N, ^{13}C, 85% ^2H)-labeled sample. The triple resonance experiments included HNCA, HN(CO)CA, HN(CA)CO, and HNCO. Backbone amide resonance assignments were confirmed using a 3D ^{15}N-edited NOESY-TROSY-HSQC spectrum (τ_{NOE} = 200 ms), which was recorded on a 750 MHz spectrometer using (^{15}N, ^2H)-labeled sample. Protein aliphatic and aromatic resonances were assigned using a combination of 2D ^{13}C HSQC, 3D ^{15}N-edited NOESY-TROSY (τ_{NOE} = 120 ms) and ^{13}C-edited NOESY-HSQC (τ_{NOE} = 150 ms) recorded on a 900 MHz spectrometer. These experiments were performed using a (^{15}N, ^{13}C)-labeled protein samples in deuterated bicelles, i.e., the acyl chains of DMPC and DHPC were deuterated (Anatrace). Specific stereo assignment of the methyl groups of valines and leucines were obtained from a 28 ms constant-time ^1H-^{13}C HSQC spectrum recorded using a 15% ^{13}C-labeled sample (Szyperski et al., 1992). Assignments of the backbone NH and sidechain methyl groups are shown in Figures 1B, 1D, S2A, and S2B.

Backbone Chemical Shift and TALOS Analyses

The assigned chemical shift values of backbone ^{15}N, $^{13}C\alpha$, and $^{13}C'$ were used as input for the TALOS+ program (Shen et al., 2009) for predicting backbone dihedral angles. Out of 32 residues with assignments, the dihedral angles of 28 residues were considered by TALO+ as 'GOOD'. Furthermore, the $^{13}C\alpha$ secondary shifts of DR5^{TMH} and the G217Y mutant are shown in Figure S2C, providing a secondary structure mapping of the TM fragment.

Assignment of NOE Restraints

Intramolecular distance restraints derived from nuclear Overhauser enhancements (NOEs) were obtained from the above-mentioned ^{15}N-edited and ^{13}C-edited NOESY spectra recorded on a 900 MHz spectrometer. Determining the inter-protomer distance restraints faced the challenge of measuring NOEs between structurally equivalent protomers having the same chemical shifts. To solve this problem, we prepared a mixed sample in which half of the protomers were ^{15}N, ^2H-labeled (0.4 mM) and the other half 15% ^{13}C-labeled (0.4 mM). Recording a 3D ^{15}N-edited NOESY-TROSY-HSQC (τ_{NOE} = 200 ms) on this sample allowed measurement of

exclusive NOEs between the ^{15}N-attached protons of one subunit and aliphatic protons of the neighboring subunits. The non-deuterated protein was 15% ^{13}C-labeled for recording the ^{1}H-^{13}C HSQC spectrum as internal aliphatic proton chemical shift reference. Inter-protomer NOE strips of the WT DR5^{TMH} is shown in Figure 2A.

To distinguish trimer-specific NOEs from the dimer-specific NOEs, the same mixed NOE experiment above was performed for the G217Y mutant. As shown in Figure 2B, the dimer-specific NOEs have vanished. In parallel, a control sample of the G217Y mutant with only (^{15}N, ^{2}H)-labeled protein (0.4 mM) was used to record an identical 3D ^{15}N-edited NOESY-TROSY-HSQC (Figure 2C). Comparison of the mixed and control spectra allows rigorous confirmation that a particular inter-protomer NOE was due solely to the mixing of protomers and NOT to incomplete deuteration of the protein.

Structure Calculation

Structure was calculated using the program XPLOR-NIH (Schwieters et al., 2003). We first determined the trimer structure of the G217Y mutant. The monomer structure was derived using intramonomer restraints and backbone dihedral restraints, determined from chemical shifts using the TALOS+ program (Shen et al., 2009). Using the monomer structure and inter-protomer NOEs from the mutant spectrum, the trimer assembly solution was derived using the ExSSO program (Yang et al., 2017). The unique trimer solution was then fed to XPLOR-NIH for further refinement against all NOE restraints (intra- and inter- protomer NOEs) and dihedral restraints. For each inter-protomer restraint between two adjacent protomers, three identical distance restraints were assigned respectively to all pairs of neighboring protomers to satisfy the condition of C3 rotational symmetry. The XPLOR refinement used a simulated annealing (SA) protocol in which the temperature in the bath was cooled from 1000 to 200 K with steps of 20 K. The NOE restraints were enforced by flat-well harmonic potentials, with the force constant ramped from 2 to 30 kcal/mol Å^{-2} during annealing. Backbone dihedral angle restraints were taken from the 'GOOD' dihedral angles from TALOS+, all with a flat-well (±the corresponding uncertainties from TALOS+) harmonic potential with force constant ramped from 5 to 1000 kcal/mol rad^{-2}. A total of 100 structures were calculated and 15 lowest energy structures were selected as the final structural ensemble (Figure S3; Table S2).

To calculate the dimer-of-trimer structure of the WT DR5^{TMH}, the trimer-specific inter-protomer NOEs, which are almost the same as those of the G217Y mutant, were first used to generate a trimer structure using the ExSSO program (Yang et al., 2017). Then, two copies of the trimer structure, or the hexamer, were used as input to XPLOR-NIH for further calculation to satisfy both trimer- and dimer-specific inter-protomer NOEs restraints. The XPLOR protocol used was the same as above. A total of 100 structures were calculated and 15 lowest energy structures were selected as the final structural ensemble of the dimer-of-trimer (Figures S4A and S4B; Table S2).

Analysis of Transmembrane Partition of the Trimeric Mutant of DR5^{TMH}

A previously published Paramagnetic Probe Titration (PPT) method (Piai et al., 2017a; Piai et al., 2017b) was used to determine the transmembrane partition of the trimeric DR5^{TMH} mutant in bicelles. This method is based on the notion that if the bicelle is sufficiently wide ($q > 0.5$), the lateral solvent paramagnetic relaxation enhancement (PRE) becomes negligible, thus allowing the use of measurable solvent PRE to probe residue-specific depth immersion of the protein in the bilayer region of the bicelle. We reconstituted the G217Y mutant in bicelles with $q = 0.6$ (Figure 4C) to perform the PPT as described previously (Piai et al., 2017b). The water-soluble and membrane-inaccessible paramagnetic agent, Gd-DOTA (Sigma), was used to generate solvent PREs. Gd-DOTA (in 200 mM stock solution) was titrated into the bicelle sample to reach final concentrations of 0.0, 1.0, 2.0, 4.0, 8.0, 10.0, 15 and 20 mM. At each concentration, a 2D ^{1}H-^{15}N TROSY-HSQC spectrum was recorded at 600 MHz to measure residue-specific PRE, defined here as the ratio of peak intensity in the presence (I) and absence (I_0) of the paramagnetic agent. For each of the residues, we used *Origin* (OriginLab, Northampton, MA) to fit the PRE titration curve to exponential decay

$$\frac{I}{I_0} = 1 - PRE_{amp}\left(1 - e^{-[Gd-DOTA]/\tau}\right) \quad (1)$$

to derive the residue-specific PRE amplitude (PRE$_{amp}$) (Figure S4D). To determine the position of the trimer relative to the bilayer center, we calculated, for each residue *i*, the distance (r_z) along the protein symmetry axis, which is parallel to the bilayer normal, from the amide proton to an arbitrary reference point based on the structure of the DR5^{TMH} mutant trimer. This calculation converted PRE$_{amp}$ versus (residue number) to PRE$_{amp}$ versus r_z (Figure S4E), which was then analyzed using *the sigmoidal fitting* method. Briefly, the trimer structure was moved along the 3-fold axis in increment of 0.3 Å (Figure S4F) to achieve the best fit to the symmetric sigmoid equation

$$PRE_{amp} = PRE_{amp}^{min} + \frac{\left(PRE_{amp}^{max} - PRE_{amp}^{min}\right)}{1 + e^{\left(r_z^I - |r_Z|\right)/SLOPE}}, \quad (2)$$

where PRE_{amp}^{min} and PRE_{amp}^{max} are the limits within which PRE$_{amp}$ can vary, r_z^I is the inflection point (the distance from the bilayer center at which PRE$_{amp}$ is halfway between PRE_{amp}^{min} and PRE_{amp}^{max}), and SLOPE is a parameter which reports the steepness of the curve at the inflection point. The best fit gave an adjusted coefficient of determination (R^2_{adj}) of ~0.9 (Figure S4F), and was used to determine the position of the trimer structure with respect to the bilayer center ($r_z = 0$).

TRAIL Preparation

TRAIL was prepared as described (Ashkenazi et al., 1999). DNA encoding the human TRAIL (residues 114-281) was synthesized by Genescript and subcloned into the pET28a (+) vector. The plasmid was transformed into *E. coli* strain BL21 (DE3) cells for protein expression. The cells were grown in LB medium supplemented with 50 μg/ml kanamycin. Cultures were grown at 37°C to an absorbance of ~0.6 at 600 nm, and cooled to 28°C, followed by overnight induction with 100 μM isopropyl β-D-thiogalatopyranoside (IPTG) at 28°C. The cells were lysed in the *Lysis Buffer* (100 mM NaH_2PO_4, 350 mM NaCl, pH 7.4). TRAIL was purified from the soluble lysate by Ni-NTA affinity chromatography in the Lysis Buffer, supplemented with 150 mM imidazole for elution. Ammonium Sulfate was added to TRAIL elution from Ni-NTA to a final concentration of 0.4 M. The elution was loaded to Hitrap phenyl FF column (GE, hydrophobic interaction chromatography (HIC) column) pre-equilibrated in the *FPLC Buffer* (100 mM NaH_2PO_4, 350 mM NaCl, 0.4 M $(NH_4)_2SO_4$, pH 7.4). The elution fractions containing pure TRAIL were collected, pooled and exchanged into the PBS buffer (pH 7.4) using PD10 column (GE). Purified TRAIL solution was concentrated by centricon (10 kDa cut-off, Millipore), filtered (0.22 μm) and stored at −80°C before use.

Ligand-Induced DR5 Activation Assay Using DR5-Expressing Stable Cell Line

Full-length human DR5 cDNA encoding isoform 1 (NCBI Ref. NP_003833.4) was cloned into the pVCR8400-Puro vector (gift from the Springer Lab) to generate the plasmid for expressing the WT DR5. Plasmids with mutations (G217Y, A222Y, A222Y/G217Y or V227Y) were prepared by site-directed mutagenesis based on the WT DR5 plasmid. These plasmids were used with the HEK293T cells to establish DR5-expressing stable cell lines. Briefly, 48 h after transfection, cells were treated with 2 μg/mL puromycin. Clonal populations were produced by limited dilution, and individual clones were screened for DR5 surface expression. FITC-labeled anti-DR5 antibody was used to evaluate cell surface expression level of DR5 by flow cytometry (ACEA NovoCyte, ACEA Biosciences) (Figure S5B).

In vitro efficacy study was performed on the monoclonal stable HEK293T cells with similar DR5 (or mutant) expression level. Cells were seeded at 10^4 per well in 96-well plates. On the morrow, adherent cells were incubated with serial concentrations of TRAIL (DR5 ligand) for 12 h to allow full cytotoxic effect of TRAIL. Ultimately, cells were incubated with 10% (v/v) Cell count kit (CCK-8, Dojindo) agent for about 1 h. Absorbance at 450 nm was measured by using the BioRad Model 680 Microplate Reader. IC_{50}, defined as the concentration of TRAIL that reduced the response of untreated control group by half, was calculated using GraphPad Prism 6.01.

Cell Imaging

WT or mutant DR5-EGFP constructs were transfected into DR5-defficient BJAB cells by electroporation as described above. Twelve hours post-transfection, cells were transferred to glass-bottomed dishes pretreated by poly-glycine and then stained by Hoechst for 1 hour for nucleus staining. All the images were taken under Olympus Fluoview FV1000 confocal microscope (Figure S6A).

DR5-EGFP, TEV-cleavable DR5-EGFP, and the mutant DR5-EGFP (G217Y) constructs (0.6 μg) were transfected into 2.0×10^6 HEK293T cells in a 35 mm glass bottomed dishes (MatTek corporation) by lipofectamine 2000 (Invitrogen). Eight hours post-transfection, cells were stained by Hoechst for 1 hour for nucleus staining and imaging. For TEV cleavage assay and TRAIL stimulation assay, cells were treated by 100 μg/ml TEV enzyme or 250 ng/ml TRAIL for another 2 hours before imaging. All the images were taken under Olympus Fluoview FV1000 confocal microscope (Figure S6B).

Ligand-Induced DR5 Activation Assay Using Transiently Transfected Cells

The same full-length human DR5 was cloned into the pcDNA3-GFP-LIC vector (a gift from Scott Gradia (Addgene plasmid # 30127)) using ligation independent cloning for expression of C-terminal GFP-tagged DR5. All DR5 mutants were generated by site-directed mutagenesis. 2 μg plasmids of the WT, DR5-TEV and mutant DR5 were transfected into 2.0×10^6 DR5-deficient BJAB cells (gift from Dr. Thorburn) by electroporation using cell line nucleofector Kit V (Lonza). 14 h post-transfection, cells were treated with TRAIL ligand for 5 h and then analyzed for active Caspase-8 using the CaspGLOW red Caspase-8 activity kit (Biovision) and flow cytometry (BD FACSAria II) (Figures 5B and S5A). Caspase-8 inhibitor IETD-FMK was conjugated to sulfo-rhodamine (Red-IETD-FMK, or DsRed2) as the fluorescent *in situ* marker to label apoptotic cells. The 561 nm laser with 585/42 band pass (BP) emission filter was used for DsRed2, and the 488 nm laser was used to excite the GFP and measured with a 520/20 BP filter.

Fluorescence Resonance Energy Transfer

In the Fluorescence Resonance Energy Transfer (FRET) assay, the intracellular fragment of DR5 was replaced by ECFP or EYFP. Truncated DR5 cDNAs encoding residues 1 – 245 (WT and mutants) was cloned into the pECFP-N1 or pEYFP-N1 vector (Clontech Laboratories). After confirmation of DR5 sequences and expression, the YFP and CFP fused DR5 variants were co-transfected into the HEK293T cells. Empty pECFP-N1 and pEYFP-N1 vectors were also co-transfected into the HEK293T cells for FRET negative control. Then, 48 h after transfection, cells were treated with 10 μg/mL TRAIL or PBS for 4 h, followed by fixation with 4% paraformaldehyde before the FRET assay. Acceptor photobleaching experiments were performed using the Nikon A1 confocal microscope (FV3000-fluoview) with 40 mW argon lasers. CFP (donor) and YFP (acceptor) were excited with 405 nm and 515 nm lasers, respectively. Before YFP channel bleaching, both CFP and YFP channels were excited to obtain pre-bleaching FRET signal. Cells were examined with a 60 × oil-immersion objective lens and bleached in the YFP channel to analyze region of interest (ROI, e.g., plasma membrane bound DR5) using the 515 nm laser at 100% intensity (95 Mw laser power). Bleaching lasted 2 to 4 s, depending on the

locations of bleached ROIs. CFP images were acquired to calculate FRET efficiency. Fifteen-eighteen images in the CFP channel were taken per ROI after photobleaching. At least 10 ROIs were used for each sample (n > 10). FRET efficiency ($FRET_{eff}$) was quantified as $FRET_{eff} = (D_{post}-D_{pre})/D_{post}$, where D_{post} is the fluorescence intensity of the Donor (DR5-CFP) after acceptor (DR5-YFP) photobleaching, and D_{pre} is the fluorescence intensity of the Donor before acceptor photobleaching.

Apoptosis Induced by TEV Cleavage-Mediated DR5 ECD Removal

TEV cleavage sequence (ENLYFQGGGGGS) was introduced into the linker region between the ECD and TMH of human DR5 isoform 1 after residue 208. The TEV cleavage construct (DR5-TEV) was transfected into DR5-deficient BJAB cells by electroporation. The DR5 with TEV cleavage sequence can also be activated by TRAIL and showed similar sensitivity to TRAIL (Figure 6B). 14 h after transfection, cells were treated with 10, 20, 40, or 100 μg/ml TEV enzyme for 5 h at 37°C. The TEV-treated cells were analyzed for active Caspase-8 using the CaspGLOW red Caspase-8 activity kit and flow cytometry (BD FACSAria II). The 561 nm laser with 585/42 band pass (BP) emission filter was used for DsRed2, and the 488 nm laser was used to excite the GFP and measured with a 520/20 BP filter.

For activation of TNFR2 (Figure 7B) and OX40 (Figure 7C) by proteolytic removal of the ECD in the absence of ligands, TEV cleavage sequence (ENLYFQGGGGGS) was introduced into the linker region between the ECD and TMH for human TNFR2/OX40. In 24-well plates, 20 μg of NF-κB plasmid (pHAGE-NF-κB, a gift from Darrell Kotton; Addgene plasmid # 49343) and 50 μg of plasmid of the TEV-cleavable TNFR2/OX40 or the WT TNFR2/OX40 were co-transfected into HEK293T cells using Lipofectamine 3000 (Invitrogen). 14 h after transfection, cells were treated with 10, 40, or 100 μg/ml TEV enzyme for 5 h at 37°C. The cell lysates of TEV-treated cells were analyzed for luminescence using the Dual-Luciferase Reporter Assay kit (Promega). Normalized relative luminescence is calculated as the difference between luminescence of the TEV-treated and non-TEV treated cell lysate divided by the cell lysate input (mg/ml). Results were from 3 independent experiments (n = 3), and expressed as mean ± SEM.

TEV Cleavage Validation by Flow Cytometry

TEV-treated cells were washed with PBS buffer 3 times and incubated with primary anti-DR5 monoclonal antibodies (R&D systems, catalog number: mab631) for 30 min on ice. Then the cells were washed 3 times with cold PBS, followed by incubation with Alexa Fluor-647 conjugated secondary antibodies (Abcam) for 30 min on ice. The cells were washed again with cold PBS 3 times and analyzed by flow cytometry (BD FACSAria II) (Figures S7A and S7B). The 633 nm laser with 670/20 band pass (BP) emission filter was used for Alexa fluor 647, and the 488 nm laser was used to excite the GFP and measured with a 520/20 BP filter.

QUANTIFICATION AND STATISTICAL ANALYSIS

Statistical significance was calculated by using GraphPad Prism 6.01 (unpaired Student's test). The number of independent experiment of duplicates, the statistical significance, and the statistical test used to determine the significance are indicated in each figure or figure legend or method section where quantification is reported.

DATA AND SOFTWARE AVAILABILITY

The atomic structure coordinate and structural constraints have been deposited in the Protein Data Bank (PDB), accession numbers PDB: 6NHW (WT) and PDB: 6NHY (mutant). The chemical shift values have been deposited in the Biological Magnetic Resonance Data Bank (BMRB), accession numbers 30553 (WT) and 30554 (mutant).

Cell

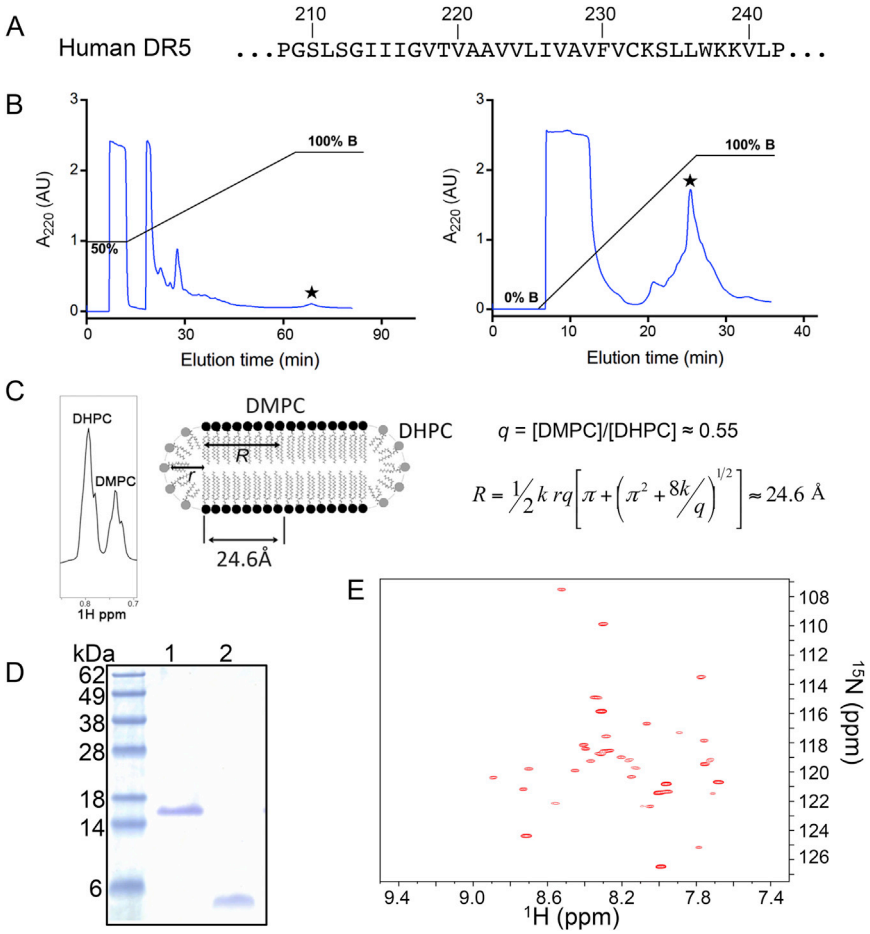

Figure S1. Purification and Reconstitution of Human DR5^{TMH}, Related to Figure 1

(A) Amino acid sequence of the TM fragment of human DR5 (isoform 1) used in the current study.

(B) Two-step HPLC protocol needed to purify DR5^{TMH}, which is unusually hydrophobic with a GRAVY index of 1.7 (calculated using the ExPASy protparam tool). *Left*: First gradient elution from 50% - 100% Buffer B in 1 h. Black star labeled peak indicates DR5^{TMH} peak. *Right*: Second gradient elution from 0% - 100% Buffer B in 30 min. Buffer A: 5% (v/v) isopropanol, 95% H_2O, 0.1% (v/v) trifluoroacetic acid (TFA); Buffer B: 75% (v/v) isopropanol, 25% acetonitrile, 0.1% (v/v) TFA.

(C) Bicelle reconstitution. *Left*: ^{1}H 1D spectrum of the NMR sample of DR5^{TMH} indicates that the molar ratio of DMPC to DHPC (*q*) of the bicelle is ~0.57. *Middle*: Schematic illustration of an ideal DMPC-DHPC bicelle. *R* and *r* are the radii of the planar region and the rim, respectively. *Right*: The equation describing *R* as a function of *q* (Glover et al., 2001; Wu et al., 2010), where r = 20 Å and k = 0.6 is the ratio of headgroup density of DMPC to that of DHPC.

(D) SDS-PAGE analysis of DR5^{TMH}. Adapted from Figure 2D. The gel lanes are: (1) WT DR5^{TMH} reconstituted in DMPC-DHPC bicelles; (2) purified DR5^{TMH} powder dissolved in gel loading buffer (not reconstituted). Samples were not boiled before SDS-PAGE.

(E) ^{1}H-^{15}N TROSY-HSQC spectrum of (^{15}N, ^{13}C, ~85% ^{2}H)-labeled DR5^{TMH} reconstituted in DMPC-DHPC bicelles (q = 0.55), recorded at 30°C and 600 MHz.

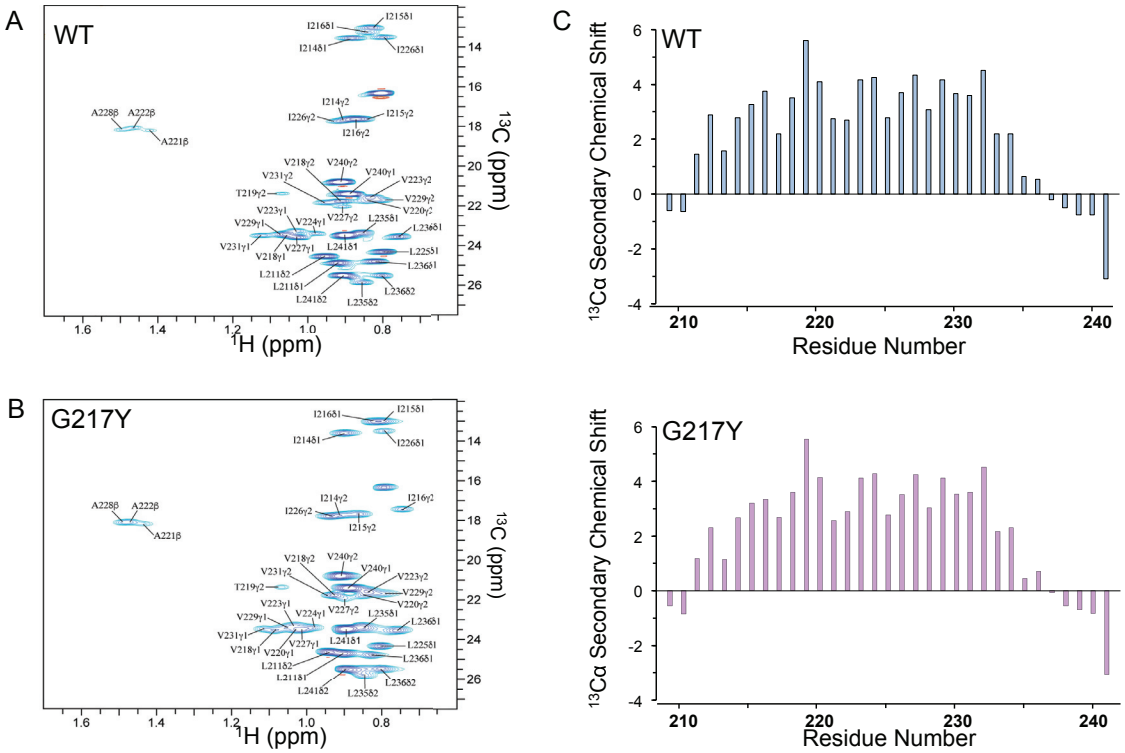

Figure S2. Assigned NMR Spectra of DR5 TMHs in Bicelles, Related to Figure 2

(A) Spectra of the WT DR5^{TMH}. The ^{1}H-^{13}C HSQC (28 ms ^{13}C constant time) recorded at ^{1}H frequency of 750 MHz using (^{15}N, ^{13}C)-labeled protein. The proteins were reconstituted in DMPC-DHPC bicelles (q = 0.55), in which the acyl chains of DMPC and DHPC were deuterated.

(B) Spectra of the G217Y mutant recorded in the way as in (a) but at 800 MHz. The labels with apostrophe indicate the presence of a minor population for residues close to the N terminus.

(C) Comparison of the ^{13}Ca secondary chemical shifts between the WT (light blue) and the G217Y mutant (red) reconstituted in bicelles with q = 0.55. The secondary chemical shift values were generated using the program TALOS+ (Shen et al., 2009).

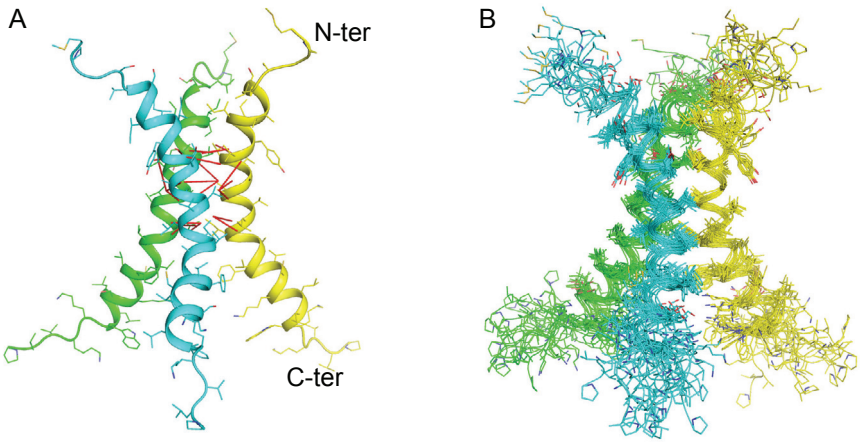

Figure S3. Inter-Protomer Restraints and Structural Convergence of the G217Y Mutant of DR5^{TMH}, Related to Figure 3

(A) Ribbon representation of the trimer structure showing NOE-derived inter-protomer restraints (red lines).

(B) Ensemble of 15 lowest energy structures calculated using NMR-derived structural restraints (see Table S2). Structures are shown as thin ribbon representation of the backbones and stick representation of the side chains.

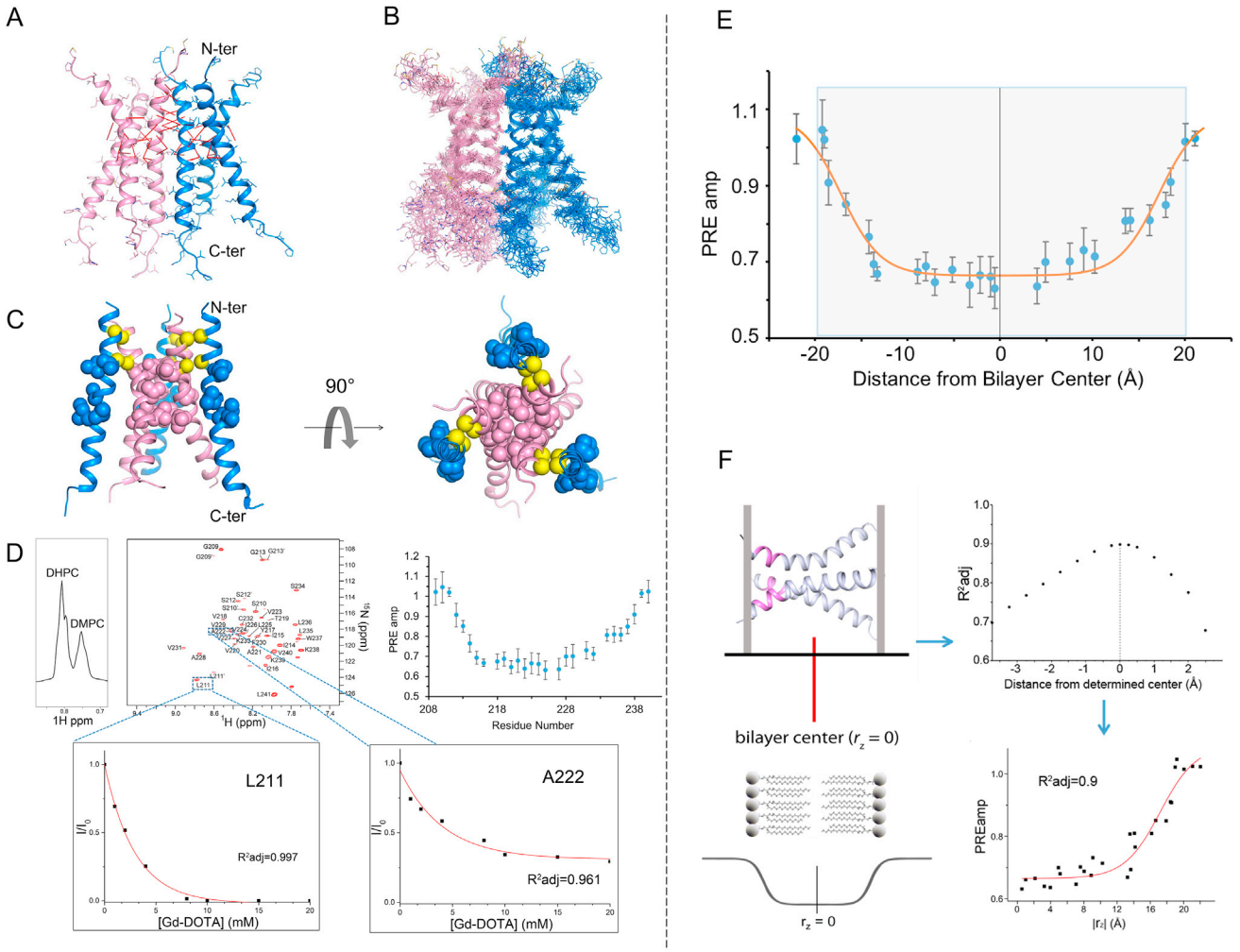

Figure S4. Inter-Protomer Restraints and Structural Convergence of the WT DR5^{TMH} Dimer-of-Trimer, the Trimer-of-Dimer Structure, and Transmembrane Partition of the G217Y Mutant in Bicelles, Related to Figure 4

(A) Ribbon representation of the trimer structure showing NOE-derived inter-protomer restraints across both dimer and trimer interfaces (red lines).

(B) Ensemble of 15 lowest energy structures calculated using NMR-derived structural restraints. Structures are shown as thin ribbon representation of the backbones and stick representation of the side chains.

(C) Ribbon representation of the trimer-of-dimer structure of WT DR5^{TMH} calculated using the same NMR data used to derive the dimer-of-trimer structure (Figure 4A). Residues involved in the trimer-specific inter-protomer contacts are highlighted (side chain heavy atoms shown as spheres). In addition, the Cα atoms of G213 and G217 are shown as yellow spheres.

(D) *Left*: 1D ^{1}H spectrum of the bicelle sample recorded at 600 MHz, showing that the peak intensity ratio of the DMPC terminal methyl groups to that of the DHPC terminal methyl groups is 0.6 (or $q = 0.6$). *Middle*: PRE versus [Gd-DOTA] for L211 and A222, measured with a series of ^{1}H-^{15}N TROSY-HSQC spectra recorded at different Gd-DOTA concentrations. The data were fitted to the exponential decay function (Equation 1) to determine the PRE amplitude (PRE_{amp}). The PRE is defined as the ratio of peak intensity in the presence (I) and absence (I_0) of Gd-DOTA. *Right*: Complete plot of PRE_{amp} versus residue number.

(E) Plot of PRE_{amp} versus distance after the positions of the backbone HN are calculated from the trimer structure of the mutant.

(F) Assignment of the bilayer center to the trimer structure by data fitting. Left: Illustration for showing the sliding of the TMH structure along the 3-fold axis (or bilayer normal) to yield best fit to the symmetric sigmoidal function (Equation 2). The $r_z = 0$ of the sigmoidal function corresponds to the bilayer center. Right upper: The adjusted coefficient of determination (R^2_{adj}) from data fitting versus deviation from the true bilayer center. The plot shows that R^2_{adj} is a reliable indicator of the protein position with an error of about ± 0.1 Å. Right lower: The best fit of the PRE_{amp} versus r_z data to the symmetric sigmoidal function. The same fit is shown in (D).

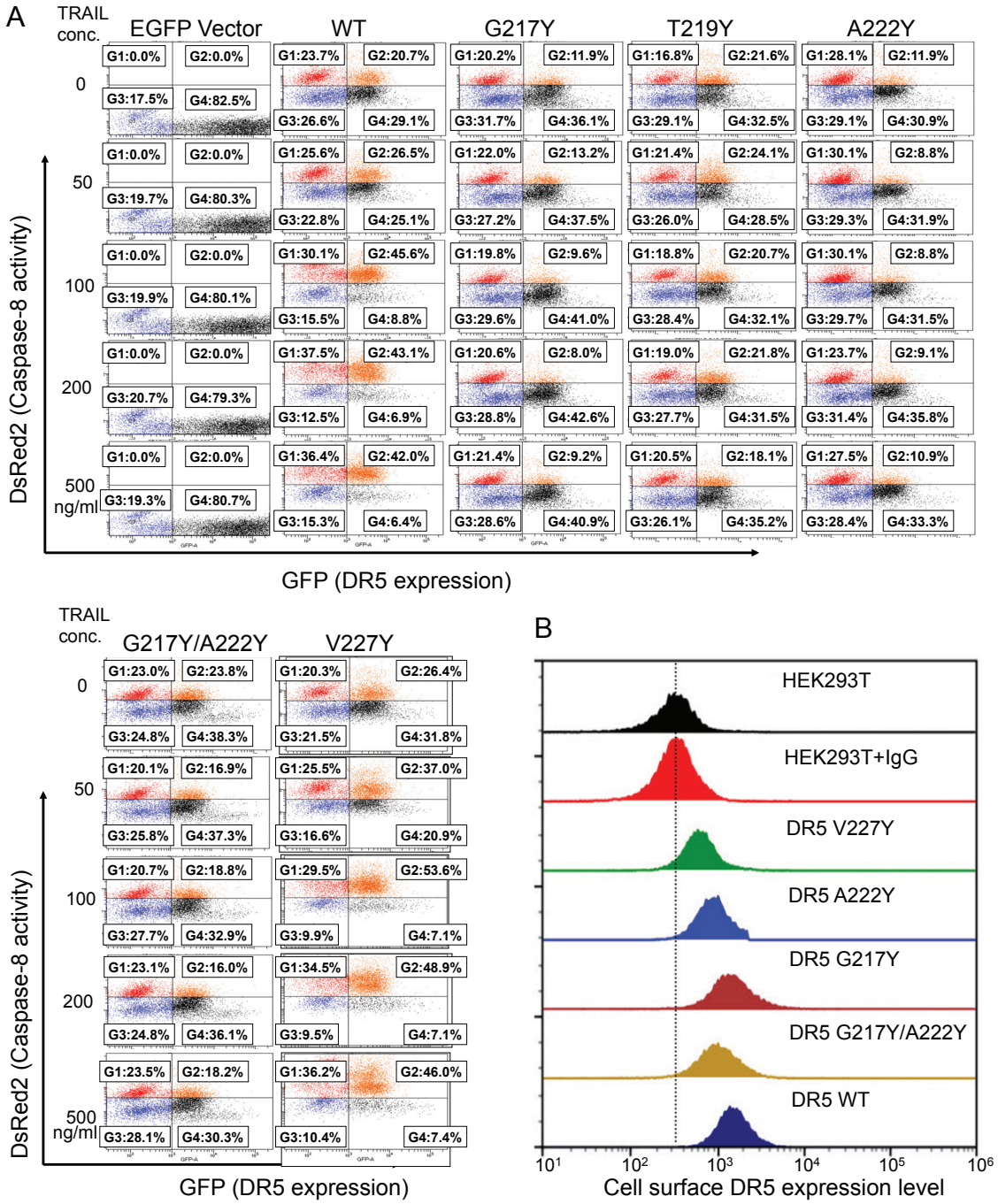

Figure S5. Raw Data of Receptor Surface Expression and TRAIL-Induced Apoptosis, Related to Figure 5

(A) Representative flow cytometry results of the TRAIL-induced apoptosis assay using transient transfection of DR5 variants. DR5 variants fused with C-terminal GFP were transiently expressed in DR5-deficient BJAB cells. CaspGLOW Red Active Caspase-8 Staining Kit utilizes the Caspase-8 inhibitor IETD-FMK conjugated to sulfo-rhodamine (Red-IETD-FMK, or DsRed2) as the fluorescent *in situ* marker. The 561 nm laser with 585/42 band pass (BP) emission filter was used for DsRed2, and the 488 nm laser was used to excite the GFP and measured with a 520/20 BP filter. Flow cytometry was performed on BD FACSAria II. Gate 1 (G1) represents DsRed2+ cells; Gate 2 (G2) represents DsRed2+/GFP+ cells; Gate 3 (G3) represents negative cells; Gate 4 (G4) represents GFP+ cells. Cell population percentage is labeled in each gate. Transfection efficiency was calculated as the sum of the percentages in G2 and G4. Caspase-8 activity was calculated as 100% × G2 / (G2+G4). Expression level of DR5 and its mutants can be estimated with DR5-GFP positive cell population, which consists of G2 and G4 percentages.

(B) Comparison of cell surface expression levels of the various monoclonal DR5 (WT and mutants) in HEK293T cells (stable cell lines). FITC-labeled anti-DR5 antibody was used to quantitate the cell surface expression level of DR5 by flow cytometry (ACEA NovoCyteTM, ACEA Biosciences). HEK293T cells treated with irrelevant IgG were used as negative control. Overall, the monoclonal DR5-expressing HEK293T cells showed similar cell surface expression for DR5 and mutants.

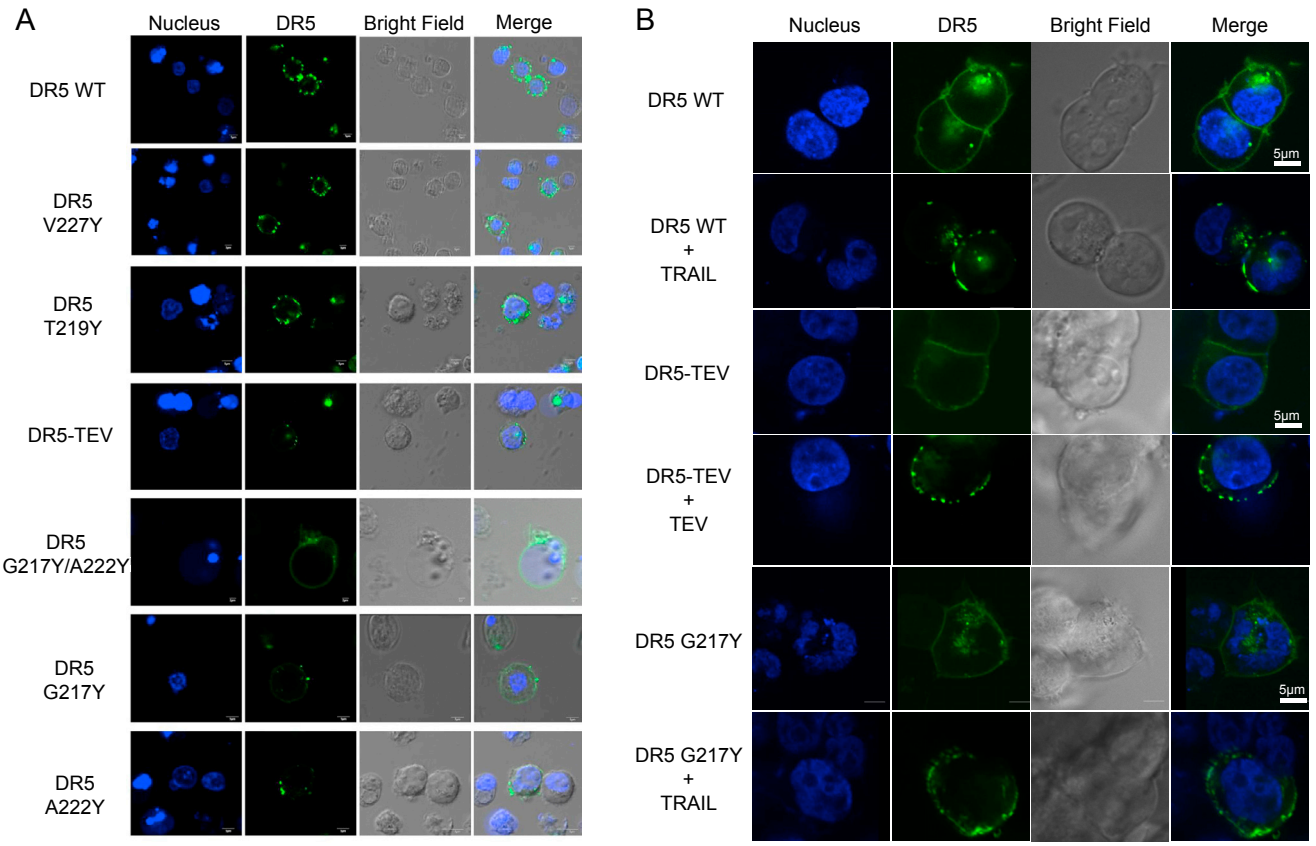

Figure S6. Analysis of Receptor Distribution on the Cell Surface by Confocal Microscopy, Related to Figure 5

(A) Confocal images of DR5-deficient BJAB cell expressing DR5-EGFP (DR5 with C-terminal fused EGFP) or its variants. The images were taken 12 hours after transfection. As can be seen, DR5-EGFP variants were mostly expressed on the plasma membrane. Related to Figure 5.

(B) Confocal images showing the distributions of DR5-EGFP and variants on cell surface before and after ligand or enzyme treatment. In glass bottomed dishes, HEK293T cells were transiently transfected with WT DR5-EGFP or TEV-cleavable DR5-EGFP, or the corresponding dimer-breaking mutant (G217Y). Eight hours post-transfection, cells were stained by Hoechst for 1 hour for nucleus staining and imaging. For TEV cleavage assay and TRAIL stimulation assay, cells were treated with TRAIL or TEV for another 2 hours.

All the images in (A) and (B) were taken using the Olympus Fluoview FV1000 confocal microscope.

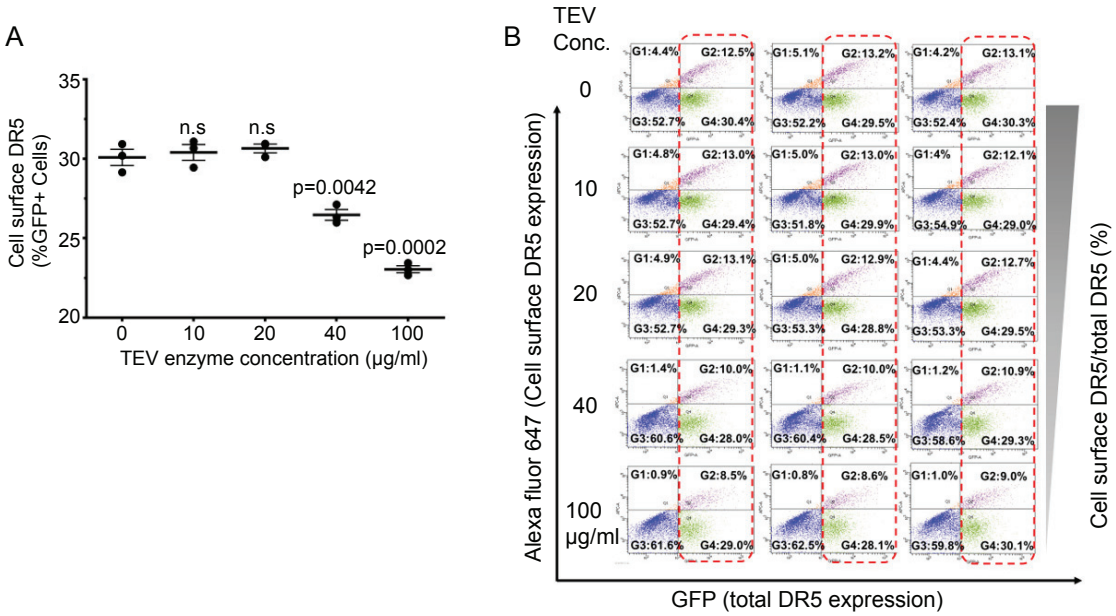

Figure S7. Removal of ECD by TEV Cleavage and Receptor Activation, Related to Figure 6

(A) Quantification of cell surface DR5 after TEV treatment. After TEV treatment, cells were immunostained with anti-DR5 primary antibodies and Alexa Fluor 647 conjugated secondary antibodies and analyzed by flow cytometry. Results are from 3 independent experiments (n = 3), and expressed as mean ± SEM. The unpaired Student's test was used to compare differences between two groups.

(B) Raw flow cytometry images of (A), which confirms TEV cleavage of DR5-TEV extracellular domain (ECD) by flow cytometry (BD FACSAria II). TEV-treated cells were immunostained by anti-DR5 monoclonal antibodies after TEV treatment, followed by flow cytometry analysis. The 633 nm laser with 670/20 band pass (BP) emission filter was used for Alexa fluor 647, and the 488 nm laser was used to excite the GFP and measured with a 520/20 BP filter. Gate 1 (G1) represents Alexa fluor 647+ cells; Gate 2 (G2) represents Alexa fluor 647+ /GFP+ cells; Gate 3 (G3) represents negative cells; Gate 4 (G4) represents GFP+ cells. Cell population percentage is labeled in each gate. Transfection efficiency is G2+G4.